Systems/Circuits

From Receptive to Perceptive Fields: Size-Dependent Asymmetries in Both Negative Afterimages and Subcortical On and Off Post-Stimulus Responses

Xu Liu,[1,3] Hui Li,[1] Ye Wang,[4] Tianhao Lei,[1] Jijun Wang,[5] Lothar Spillmann,[6*] Ian Max Andolina,[1,2] and Wei Wang[1,2,3]

[1]Institute of Neuroscience, Center for Excellence in Brain Science and Intelligence Technology, State Key Laboratory of Neuroscience, Key Laboratory of Primate Neurobiology, Chinese Academy of Sciences, Shanghai, 200031, China, [2]Shanghai Center for Brain and Brain-inspired Intelligence Technology, Shanghai, 200031, China, [3]University of Chinese Academy of Sciences, Beijing, 100049, China, [4]State Key Laboratory of Media Convergence and Communication, Neuroscience and Intelligent Media Institute, Communication University of China, Beijing, 100024, China, [5]Shanghai Mental Health Center, Shanghai Jiaotong University School of Medicine, Shanghai Key Laboratory of Psychotic Disorders, Shanghai, 200030, China, and [6]Department of Neurology, University of Freiburg, Freiburg, 79085, Germany

Negative afterimages are perceptual phenomena that occur after physical stimuli disappear from sight. Their origin is linked to transient post-stimulus responses of visual neurons. The receptive fields (RFs) of these subcortical ON- and OFF-center neurons exhibit antagonistic interactions between central and surrounding visual space, resulting in selectivity for stimulus polarity and size. These two features are closely intertwined, yet their relationship to negative afterimage perception remains unknown. Here we tested whether size differentially affects the perception of bright and dark negative afterimages in humans of both sexes, and how this correlates with neural mechanisms in subcortical ON and OFF cells. Psychophysically, we found a size-dependent asymmetry whereby dark disks produce stronger and longer-lasting negative afterimages than bright disks of equal contrast at sizes $>0.8°$. Neurophysiological recordings from retinal and relay cells in female cat dorsal lateral geniculate nucleus showed that subcortical ON cells exhibited stronger sustained post-stimulus responses to dark disks, than OFF cells to bright disks, at sizes $>1°$. These sizes agree with the emergence of center-surround antagonism, revealing stronger suppression to opposite-polarity stimuli for OFF versus ON cells, particularly in dorsal lateral geniculate nucleus. Using a network-based retino-geniculate model, we confirmed stronger antagonism and temporal transience for OFF-cell post-stimulus rebound responses. A V1 population model demonstrated that both strength and duration asymmetries can be propagated to downstream cortical areas. Our results demonstrate how size-dependent antagonism impacts both the neuronal post-stimulus response and the resulting afterimage percepts, thereby supporting the idea of perceptual RFs reflecting the underlying neuronal RF organization of single cells.

Key words: illusion; negative afterimage; perceptive field; receptive field; retina; thalamus

Significance Statement

Visual illusions occur when sensory inputs and perceptual outcomes do not match, and provide a valuable tool to understand transformations from neural to perceptual responses. A classic example are negative afterimages that remain visible after a stimulus is removed from view. Such perceptions are linked to responses in early visual neurons, yet the details remain poorly understood. Combining human psychophysics, neurophysiological recordings in cats and retino-thalamo-cortical computational modeling, our study reveals how stimulus size and the receptive-field structure of subcortical ON and OFF cells contributes to the parallel asymmetries between neural and perceptual responses to bright versus dark afterimages. Thus, this work provides a deeper link from the underlying neural mechanisms to the resultant perceptual outcomes.

Received Jan. 29, 2021; revised July 11, 2021; accepted July 13, 2021.

Author contributions: X.L., I.M.A., and W.W. designed research; X.L. and H.L. performed research; X.L., Y.W., T.L., I.M.A., and W.W. analyzed data; X.L. and I.M.A. wrote the first draft of the paper; X.L., L.S., I.M.A., and W.W. edited the paper; Y.W., T.L., and J.W. contributed unpublished reagents/analytic tools.

This work was supported by Strategic Priority Research Program of the Chinese Academy of Sciences Grant XDB32060200 (to W.W.); Shanghai Municipal Science and Technology Major Project Grant 2018SHZDZX05 (to W.W. and I.M.A.); National Natural Science Foundation of China Grants 31861143032 (to W.W.) and 32070992 (to I.M.A.); and Shanghai Science and Technology Commission Project Grant 19411969100.

*Lothar Spillmann is on a leave of absence.

The authors declare no competing financial interests.

Correspondence should be addressed to Ian Max Andolina at i.andolina@ion.ac.cn or Wei Wang at w.wang@ion.ac.cn.

https://doi.org/10.1523/JNEUROSCI.0300-21.2021

Introduction

What appears to us an effortless task, the opening of our eyes, engages an extensive and anatomic complex network of brain areas. The first stages of visual processing differentiate bright luminance increments from dark decrements by separate ON and OFF channels in the retina and dorsal lateral geniculate nucleus (dLGN) (Schiller, 1992). Most ON and OFF cell receptive fields (RFs) are selective for stimulus size and local contrast via antagonistic interactions between center and surround (Fig. 1*A*) (Kuffler, 1953; Barlow et al., 1957; Allman et al., 1985). These interactions also impact the transient rebound responses when a nonpreferred stimulus is removed from the RF (Singer and Creutzfeldt, 1970; Jung, 1973); and they are reflected in our perceptual experience, revealing close similarities between the tuning properties of neural and perceptual RFs (Oehler, 1985; Spillmann and Werner, 1990).

For example, humans are perceptually more sensitive to luminance decrements than increments (Whittle, 1986; Komban et al., 2011, 2014), as shown by our ability to read black-on-white text faster and with fewer errors than white-on-black text (Buchner and Baumgartner, 2007). Analogous physiological differences that can be linked to such asymmetries in decrement versus increment perception have been found between OFF and ON channels. OFF-center retinal ganglion cells (RGCs) possess smaller dendritic arbors and increased tiling density, outnumbering ON-RGCs (Dacey and Petersen, 1992; Ratliff et al., 2010). Furthermore, inhibition is only found from ON-bipolar to OFF-RGCs (Chichilnisky and Kalmar, 2002; Zaghloul et al., 2003; Liang and Freed, 2010, 2012; Freed, 2017). In the dLGN and primary visual cortex (V1), OFF cells respond faster and more linearly than ON cells (Jin et al., 2008, 2011; Komban et al., 2014; Kremkow et al., 2014; Rekauzke et al., 2016); and OFF-dominated neurons in V1 show stronger responses and cover a greater cortical area (Jin et al., 2008; Yeh et al., 2009; Xing et al., 2010; Zurawel et al., 2014). This OFF channel dominance is modulated by stimulus properties, such as size, spatial frequency, and duration (Khani et al., 2018; Jansen et al., 2019; Mazade et al., 2019), with stronger inhibition elicited by large bright compared with dark stimuli in V1 (Xing et al., 2014).

The responses of ON and OFF neurons have also long been associated with the perception of afterimages, where a negative "ghost" of the original stimulus is briefly perceived after a bright or dark stimulus is quickly removed from view (Fig. 1*B*) (Bidwell, 1897; Jung, 1973; Schiller and Dolan, 1994; Schiller, 1995). Afterimages have long fascinated theorists of vision because of the clear dissociation between physical and perceptual events (Phillips, 2013). Understanding such responses provides insight into the fundamental question of how neural mechanisms, such as adaptation and center-surround antagonism, underlie our subjective perception (Macknik and Livingstone, 1998; Huang et al., 2008; Zaidi et al., 2012). Recently, we have observed that, following stimulus offset, bright afterimages were stronger and lasted longer than dark afterimages for a stimulus disk of 3° in diameter. This perceptual asymmetry was paralleled by analogous post-stimulus response differences between subcortical ON and OFF cells (Li et al., 2017).

Because changes in stimulus size alter the suppressive antagonism in early visual areas, it becomes important to evaluate how size affects perceptual afterimages and the underlying post-stimulus responses that are contingent on suppression. At present, the relationship between stimulus polarity and size at stimulus offset remains poorly understood. In this study, we conducted psychophysical experiments in human observers and single-unit electrophysiological recordings of the putative retinal afferents (S-potentials) and relay cells in cat dLGN. Specifically, we investigated whether stimulus size differentially affects the perception of bright and dark afterimages in human observers, and how it correlates with subcortical neural post-stimulus responses of ON and OFF cells. From these results, a spatiotemporal population network model of RGCs and relay cells was developed to elucidate the spatial and temporal RF differences of subcortical post-stimulus responses.

Materials and Methods

Human psychophysics

Eight subjects (aged 24-34 years; 3 females and 5 males, including 2 authors), with normal or corrected-to-normal vision and no history of psychiatric or neurologic disorders, participated in the experiments. The subjects gave written consent to the procedure in accordance with institutional guidelines and the Declaration of Helsinki. Experiments were approved by the Ethics Committee of the Institute of Neuroscience, Chinese Academy of Sciences. All stimuli were presented in an otherwise dark room using MATLAB 2020a and Psychophysics toolbox version 3.0.16 (RRID:SCR_002881) (Kleiner et al., 2007), running under Ubuntu 20.04 on a hardware-linearized 34 inch 120 Hz LCD display (Display++, Cambridge Research Systems) placed 64 cm in front of the subjects. Subjects were asked to fixate on a black cross of $0.4 \times 0.4°$ positioned in the center of the screen using the left eye while the right eye was occluded. A bright or dark disk stimulus was presented for 4 s at 1 of 6 randomly assigned parafoveal positions radially positioned 3° away from the center of fixation. The edges of the stimuli were smoothed with cubic Hermite interpolation with a σ of 0.21° to minimize any microsaccadic edge effects (Bachy and Zaidi, 2014). Eye movements and blink-related variability in afterimage perception were continuously monitored by an SR Research Eyelink 1000 eye tracker recording at 1000 Hz. We aborted any trial where subjects blinked or where fixational eye movements exceeded a circular radius around the fixation cross of 0.75°. The luminance range of the screen was defined by floating-point values between 0 and 1 where 0 indicates the lowest luminance (0.1 cd/m^2) and 1 indicates the highest luminance (120 cd/m^2). The luminance of the background was set to 0.5 (60 cd/m^2). We defined the linear steps of contrast as the difference between the stimulus luminance and the 0.5 background; the contrast of the brightest stimulus is $1 - 0.5 = 0.5$, the contrast of the background is $0.5 - 0.5 = 0$, and the contrast of the darkest stimulus is $0 - 0.5 = -0.5$.

Measurement of afterimage contrast

To measure the perceived afterimage contrast, dark (luminance value: 0) and bright (luminance value: 1) stimulus disks of 0.4°, 0.8°, 1.4°, 2°, 3°, and 6° diameter were used. Immediately after the stimulus was turned off, a variable contrast (0, ±0.05, ±0.1, ±0.15, ±0.2, ±0.25, ±0.3, ±0.35) pedestal of the same size and contrast polarity was presented in the same position. The pedestal was presented for only 400 ms to restrict the measurement to the transient (Purkinje) phase of the afterimage; thereafter, a white noise mask was presented at the same location for 1.5 s. Each pedestal contrast was repeated for 8 trials in a random order, and results were averaged. Subjects were asked to respond whether they had observed any change of the background brightness between the stimulus offset and the mask onset. Perceptual equality with the background contrast indicates that the afterimage was canceled by the opposite-polarity pedestal, resulting in a perceptual null. If there was a difference and thus no cancellation, subjects reported whether the background appeared momentarily brighter or darker. A "brighter" response suggests that the decrement pedestal used to cancel the bright afterimage of a dark stimulus was too weak, and vice versa for bright stimuli.

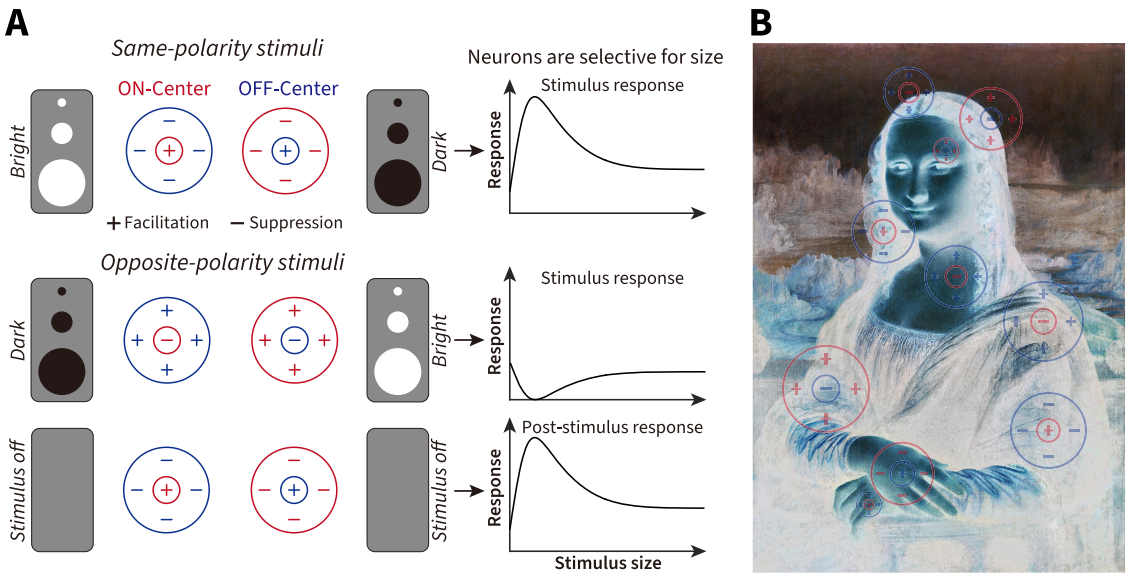

Figure 1. RF structure, stimulus size, light polarity, and negative afterimages. ***A***, Schematic of RFs and stimulus characteristics that drive size-dependent responses of ON and OFF cells. Same or opposite-polarity stimuli signify a light polarity that aligns with or is opposite to the ON- or OFF-center response. For opposite-polarity stimuli, on stimulus removal, there is a post-stimulus rebound that depends on the preceding stimulus. ***B***, Schematic of a pictorial negative afterimage that is dependent on the initial post-stimulus rebound responses of ON and OFF cells (overlaid).

Similarly, a "darker" response suggests that the increment pedestal used to cancel the dark afterimage of a bright stimulus was not strong enough, and vice versa for dark stimuli. We generated an afterimage–pedestal ratio $(N_{ped}+N_{null} \times 0.5) \div P_n$, where N_{ped} is the number of "pedestal seen" trials, N_{null} is the number of perceptual null trials, and P_n is the number of overall trials for each pedestal contrast. We fitted a Quick psychometric function of the following form:

$$PF_q = \gamma + (1 - \gamma - \lambda) - 2^{\left(-\left(\frac{x}{\alpha}\right)^{\beta}\right)}$$

where α = threshold and β = slope (γ and λ represent chance and lapse rates, respectively) using a Bayesian likelihood method with the Palamedes toolbox for MATLAB (RRID:SCR_006521) (Prins and Kingdom, 2018); we assessed the 95% CIs obtained from the posterior distributions for significance. We then formally tested for significant differences between psychometric functions using Monte Carlo simulations of the likelihood ratios for each fit (Prins and Kingdom, 2018). The natural range of the afterimage/pedestal ratio is $0 \leftrightarrow 1$ (0 signifies afterimage always seen; 1 signifies pedestal always seen).

Measurement of afterimage duration

The disks were presented for 4 s as before. After the stimulus offset, subjects were asked to report with a button-press when the afterimages disappeared. The time between stimulus offset and subject's response was taken as the afterimage duration. Each stimulus was repeated 8 times.

Measurement of afterimage masking time latency

Dark and bright disks were again presented for 4 s. After stimulus offset, subjects were asked to report whether they perceived (YES/NO) an afterimage before a variably delayed ($\Delta t = 0$, 0.05, 0.1, 0.2, 0.3, 0.4, 0.5, and 0.6 s) white noise mask presented at the same location for 1.5 s. Each condition was repeated for 8 trials in a random order. The curves of afterimage-seen proportion to delayed time were fitted by using a Bayesian likelihood method with a Quick psychometric function. The latency was measured as the value of the afterimage seen proportion first reaching 50%.

Electrophysiological recordings

Animal preparation. All experimental procedures were approved by the Animal Care and Use Committee of the Institute of Neuroscience and by the local ethical review committee of the Shanghai Institutes for Biological Sciences. Eighteen adult female cats (2-4 kg) were anesthetized and paralyzed with pentobarbital sodium and gallamine triethiodide. Artificially respiration was maintained with rate adjustments to keep end-tidal CO_2 between 3.1% and 3.6%. Body temperature was monitored to maintain near 38°C. Atropine (0.05%), gentamycin (4%), and dexamethasone (0.5%) were injected intramuscularly every 12 h to prevent secretion, infection, and brain edema, respectively. Ear bars and canals were coated with antiseptic lidocaine hydrochloride gel. All incisions were treated with lidocaine. The pupils were dilated with atropine methonitrate (2% w/v), and nictitating membranes were retracted with phenylephrine hydrochloride (2.5% w/v). Contact lenses with artificial pupils were placed in front of both eyes. Eyes were regularly checked and cleaned as necessary throughout the experiment. The locations of the optic disk and fovea were plotted using a reversible ophthalmoscope.

Recording procedures and visual stimuli. A craniotomy was performed at Horsley-Clarke coordinates A6, L8. Single-unit recordings were made in cats' dLGN A and A1 laminae using tungsten-in-glass electrodes (1-3 MΩ). Data were collected and stored by Axon CNS Multiclamp 700B and Axon CNS Digitata 1440A. S-potentials were manually sorted via Plexon Offline Sorter software. All stimuli were presented on an HP P1230 CRT monitor with a refresh rate of 85 Hz. The monitor's luminance (range: 0.1-68.5 cd/m^2) was linearized using a ColorCAL colorimeter (Cambridge Research Systems). The contrast of visual stimuli was identical to that used for the psychophysics.

A full-field flash was used to determine the response type for ON and OFF center neurons. RFs were mapped both by hand and by computing the spike-triggered average stimulus with a 16×16 grid white noise stimulus refreshed at 85 Hz. The grid element sizes vary between 0.2° and 0.4°, dependent on the RF. The RF center position was estimated using a two-dimensional elliptical Gaussian function fit to the peak of spike-triggered average (Chichilnisky and Kalmar, 2002; Gauthier et al., 2009). The RF size measured with white noise was defined as the diameter of a circle with the same area as the 3 SD boundary of a two-dimensional circular Gaussian fit to the spike-triggered average. Spatial frequency tuning was measured using drifting sinusoidal gratings of varying spatial frequency. We used 5° diameter patches of contrast-reversing sinusoidal grating stimuli with 12 phases (0°-330° with 30° steps in a randomized sequence, tested at the optimal and cutoff spatial frequency if necessary) as a null test. Along with the RF information, including potential shift effects and transient/sustained firing response profile, the cell was classified as either X or Y (Enroth-Cugell and Robson, 1966; Hochstein and Shapley, 1976; Derrington and Fuchs, 1979).

After carefully mapping the RF, dark (contrast −0.5) or bright (contrast 0.5) disk stimuli of differing size (0.2°, 0.4°, 0.6°, 0.8°, 1°, 2°, 4°, 6°, 8°, and 10°) were presented centered over the RF of each cell against a mean-luminance background (contrast 0) for a duration of 500 ms and followed by 300 ms (in 44 of 168 cells) or 1000 ms (in 124 of 168 cells) blank (contrast 0). Each stimulus size was presented 15 times in a random sequence.

Measurement of the response strength of ON and OFF cells. For same-polarity stimuli (bright disks for ON cells, dark disk for OFF cells), the stimulus response strength was measured as the average firing rate during the first 300 ms after stimulus onset. The stimulus response was corrected for baseline firing, defined as a neuron's averaged spontaneous firing rate to the background luminance alone. For opposite-polarity stimuli (bright disks for OFF cells, dark disk for ON cells), neurons were suppressed at the onset and facilitated at the offset. The suppressive effect during opposite-polarity stimulation was calculated as the baseline activity minus the firing rate during the first 300 ms after the onset of the opposite-polarity stimulus. The post-stimulus response strength was measured as the average firing rate (baseline-corrected) during the first 300 ms after opposite-polarity stimulus offset.

Measurement of the RF properties of ON and OFF cells. The RF center size and the strength of center-surround antagonism were measured from the size tuning curve of response strength described above. In such curves, RF center size is determined by the size of the disk that elicits the maximal response. To measure the strength of center-surround antagonism, we used a suppression index, defined as (1 – plateau response/optimal size response), where the plateau response was the minimum response from optimal size to largest size. A higher suppression index signifies that the cell has stronger center-surround antagonism (Ruksenas et al., 2000).

Measurement of the temporal response properties of ON and OFF cells. We quantified the sustained index from peristimulus time histograms (PSTHs) calculated with 1 ms bins to estimate the transient/sustained properties of responses across size. The sustained index was calculated as the ratio of the average response during the first 300 ms after stimulus onset/offset to the peak response of the PSTH (Piscopo et al., 2013). Both average and peak responses were baseline-corrected. A higher sustained index signifies that the response is more sustained. To compare the later part of the rebound response period after stimulus offset between ON and OFF cells, average firing rates were calculated for a time window of 700-1000 ms after the offset of the opposite-polarity stimulus.

Measurement of the response latency of ON and OFF cells. We used a standard 2 SD method to measure the response latency from PSTHs (Tasaka et al., 2018). To minimize noise variability, we used a Gaussian filter of 21 ms to smooth the PSTHs. We defined the response latency as the time at which the PSTH first reached 2 SDs above baseline for at least 5 successive bins after stimulus onset or offset. Here, the baseline was taken over 200 ms before stimulus onset or offset.

Statistical analysis

All averaged data are presented as the mean ± 1 SEM. Notches in box plots represent the 95% CI around the median. Nonparametric Wilcoxon rank-sum (unpaired) or rank-sign (paired) tests were used for two group comparisons. Where more than one group was compared (e.g., in size tuning curves), we used the Bonferroni–Holm method to correct the family-wise error rate for multiple comparisons. All statistical analysis was performed using the statistics toolbox in MATLAB 2020a.

Computational modeling

The eDOG model. The population responses were fit with a network-based firing-rate model, the extended difference-of-gaussians (eDOG) model (Mobarhan et al., 2018), to evaluate the spatiotemporal RF property of dLGN relay cells. The underlying modeling framework from Mobarhan et al. (2018) is available as a Python package (pyLGN), and was downloaded from https://pylgn.readthedocs.io/en/latest/ and run on an Ubuntu 20.04 workstation using Python version 3.7.

Mathematically, the model RF is defined by several spatiotemporal impulse–response functions. For a relay cell located at position r in the visual filed, the response to any stimulus can be found by convolving the impulse–response function with the following:

$$R_R(r,t) = \int_{\tau} d\tau \iint_{r_0} d^2 r_0 \, W_R(r - r_0, \tau) S(r_0, t - \tau)$$

Here $W_R(r,\tau)$ is the spatiotemporal impulse–response function of the cell, and the $S(r,t)$ represents the visual stimulus presented at position $r = (x,y)$ at time t. The spatial integral over r_0 goes over all two-dimensional space. For mathematical convenience, the temporal integral is set to from $\tau = -\infty to +\infty$. Because a stimulus cannot affect the response in the past, it then follows that $W_R(r, \tau<0) = 0$.

The impulse–response function W_R for dLGN relay cells is derived from the mechanistic eDOG model (Einevoll and Plesser, 2012). The relay cells receive feedforward excitation and indirect feedforward inhibition from RGCs via a spatiotemporal coupling-kernel function. The cortical feedback is ignored here.

The spatiotemporal impulse–response function of RGCs includes a DOG spatial function and a biphasic temporal function. The DOG spatial function $F(r)$ is given by the following:

$$F(r; K_1, a_1, K_2, a_2) = \frac{K_1}{\pi {a_1}^2} e^{-r^2/{a_1}^2} - \frac{K_2}{\pi {a_2}^2} e^{-r^2/{a_2}^2}$$

Where K_1 and K_2 are the amplitudes of the center and surround Gaussians, a_1 and a_2 are the corresponding width parameters.

The biphasic temporal function (Yousif and Denham, 2007; Norheim et al., 2012) $H(t)$ is given by the following:

$$H(t; \tau, B) = \begin{cases} sin(\pi t/\tau), 0 \le t \le \tau \\ B\, sin(\pi t/\tau), \tau \le t \le 2\tau \\ 0, otherwise, \end{cases}$$

where B is the weight for the second phase and τ is the duration of each phase.

The output functions are integrated at the thalamic network level via a spatiotemporal coupling-kernel function. The spatial kernel is a Gaussian function as follows:

$$f(r; b) = \frac{1}{\pi b^2} e^{-r^2/b^2}$$

where b is the Gaussian width.

The temporal kernel is a delayed exponential decay function (Einevoll and Plesser, 2002; Norheim et al., 2012) as follows:

$$h(t; \Delta, \tau_{RG}) = \frac{1}{\tau_{RG}} e^{-(t-\Delta)/\tau_{RG}} \Theta(t - \Delta)$$

where τ_{RG} is the time constant, Δ corresponds to a combined axonal and synaptic time delay, and $\Theta(t)$ is the Heaviside unit step function.

Feedforward excitation and inhibition from RGCs have their own spatiotemporal coupling kernels. The feedforward inhibitory coupling kernel has a larger Gaussian width and longer time delay than the excitatory kernel, reflecting the observed larger RF in intrageniculate interneurons and later inhibitory effect in the relay cells (Einevoll and Heggelund, 2000; Norheim et al., 2012).

Recurrent V1 network model. In order to better explain the relationship between LGN ON-/OFF-cell post-stimulus responses and their downstream perceptual outcomes, we constructed a recurrent spiking neural network model. The model contains two layers: LGN and V1. V1 contains 450 excitatory neurons and 112 inhibitory neurons, with recurrent connections between excitatory and inhibitory neurons. The connection probability between cortical neurons is shown in Table 1.

In the proposed model, the firing rate of the dLGN cells recorded in the electrophysiological experiments was transformed to Poisson spike

Table 1. Connection probability between neurons

Symbol	Description	Value
$p_b^{E\to E}$	Connection probability from E to E; ON pathway	0.005
$p_b^{E\to I}$	Connection probability from E to I; ON pathway	0.5
$p_b^{I\to E}$	Connection probability from I to E; ON pathway	0.01
$p_b^{I\to I}$	Connection probability from I to I; ON pathway	0.05
$p_d^{E\to E}$	Connection probability from E to E; OFF pathway	0.006
$p_d^{E\to I}$	Connection probability from E to I; OFF pathway	0.5
$p_d^{I\to E}$	Connection probability from I to E; OFF pathway	0.02
$p_d^{I\to I}$	Connection probability from I to I; OFF pathway	0.05

Table 2. Synaptic parameters

Symbol	Description	Value
$\bar{g}_b^{inp\to E}$	Synaptic weight from input to E; ON pathway	0.5 nS
$\bar{g}_b^{E\to E}$	Synaptic weight from E to E; ON pathway	1 nS
$\bar{g}_b^{E\to I}$	Synaptic weight from E to I; ON pathway	0.05 nS
$\bar{g}_b^{I\to E}$	Synaptic weight from I to E; ON pathway	0.5 nS
$\bar{g}_b^{I\to I}$	Synaptic weight from I to I; ON pathway	0.1 nS
$\bar{g}_d^{inp\to E}$	Synaptic weight from input to E; OFF pathway	0.5 nS
$\bar{g}_d^{E\to E}$	Synaptic weight from E to E; OFF pathway	1.1 nS
$\bar{g}_d^{E\to I}$	Synaptic weight from E to I; OFF pathway.	0.04 nS
$\bar{g}_d^{I\to E}$	Synaptic weight from I to E; OFF pathway.	0.5 nS
$\bar{g}_d^{I\to I}$	Synaptic weight from I to I; OFF pathway.	0.1 nS
E_{syn}^{E}	Reversal potential of excitatory synapse	0 mV
E_{syn}^{I}	Reversal potential of inhibitory synapse	−80 mV
τ_s	Decay time constant of synapse	20 ms

trains and used as the input to the network. The neurons in V1 are simulated by a leaky integrate and fire model. The dynamic voltage $V(t)$ of a neuron is given by the following:

$$\frac{dV(t)}{dt} = -\frac{1}{\tau_m}(V(t) - V_{rest}) + I_{syn}(t)$$

$$if\ V(t) > V_{thre},\ V(t) = V_{rest}$$

Where τ_m is resting membrane time constant, V_{rest} is resting membrane potential, V_{thre} is threshold potential, and I_{syn} is synaptic current. Here, the τ_m, V_{rest}, and V_{thre} are set to 10 ms, −70 mV, and −20 mV, respectively. The refractory period occurs after a neuron initiates firing. The refractory period for excitatory and inhibitory neurons is set to 10 and 4 ms, respectively. The synaptic current I_{syn} is simulated by single exponential function model as follows:

$$I_{syn}(t) = g_{syn}(t)\big(V(t) - E_{syn}\big)$$

$$g_{syn}(t) = \bar{g}\exp\left(-\frac{t - t_s}{\tau_s}\right)$$

where $\bar{g}$ is synaptic weight, E_{syn} is reversal potential of synapse, t_s is the spike time of presynaptic neuron, and τ_s is decay time constant. Parameter values for synapse are summarized in Table 2.

Results

Stimulus size affects perceived asymmetries between bright and dark afterimages

To estimate whether stimulus size affects the asymmetry between bright and dark afterimages in human observers, we selected 6 representative stimulus sizes (0.4°, 0.8°, 1.4°, 2°, 3°, and 6°) informed by the tuning characteristics of center and surround commonly observed in the RFs of early visual areas in cats (Jones et al., 2000) and perceptive fields of human and nonhuman primates (Oehler, 1985). Stimuli were smooth-edged bright or dark polarity disks presented for 4 s on a mean-luminance gray background, randomly presented in one of six perifoveal locations around the fixation point. We used noninvasive infrared eye-tracking to ensure that subjects did not blink, eye position remained steady, and confirmed that micro-saccades were evenly distributed across all conditions (mean number of micro-saccades comparing bright vs dark trials: $p = 0.93$, $p = 0.91$, $p = 0.76$, $p = 0.85$, $p = 0.61$, and $p = 0.27$ for 0.4°, 0.8°, 1.4°, 2°, 3°, and 6°, respectively; $N = 8$ subjects; Tukey's *post hoc* corrected ANOVA). To measure perceived afterimage contrast, once the afterimage-inducing stimulus was removed from view after 4 s, we immediately presented a variable-contrast pedestal of the same size, stimulus polarity, and position for 0.4 s, after which a dynamic white noise mask (designed to restrict perception to the transient phase of the afterimage) (Jung, 1973) was shown (Fig. 2*A*). Eight human subjects were asked to report whether the post-stimulus pedestal was brighter, darker, or identical to the background. A null contrast was defined as the pedestal contrast matching the perceived strength of the afterimage (where neither pedestal nor afterimage was perceived). A higher null contrast signifies that the afterimage had a stronger perceptual strength. Curves were fitted to the subject response data with a Quick function using a Bayesian fitting procedure, and the mean psychometric functions and resultant posterior distributions for threshold and slope for each stimulus size were plotted in Figure 2*B*. A rightward shift of the psychometric function signifies that a larger post-stimulus pedestal contrast is required to perceptually negate a more strongly perceived afterimage. As stimulus size was increased, we observed a rightward shift and steepening of the slope for bright afterimages, signifying that they were perceptually stronger than dark afterimages. Overall, two-way repeated-measures ANOVA revealed significant effects of stimulus polarity, size, and their interaction on the perceived strength of the afterimage (polarity: $F = 8.27$, $p = 0.024$; size: $F = 6.80$, $p = 1.59 \times 10^{-4}$; interaction: $F = 3.72$, $p = 0.0084$; $N = 8$ subjects). Tukey's *post hoc* tests revealed that bright afterimages produced by dark stimuli had a stronger perceptual strength than dark afterimages produced by bright stimuli for disk diameters >0.8° (Fig. 2*C*; $p = 0.88$, $p = 0.13$, $p = 0.0094$, $p = 0.0013$, $p = 0.0022$, and $p = 0.011$ for 0.4°, 0.8°, 1.4°, 2°, 3°, and 6°, respectively; $N = 8$ subjects). Using statistical comparisons between the fitted psychometric functions for bright and dark afterimage (Prins and Kingdom, 2018), both the α-threshold and β-slope parameters were significantly higher for bright afterimages compared with dark afterimages for sizes >0.8° (Fig. 2*B*; α-threshold: $p = 0.37$, $p = 0.069$ $p = 0$, $p = 0$, $p = 0$, and $p = 0.0013$; β-slope: $p = 0.36$, $p = 0.19$, $p = 0.0038$, $p = 0$, $p = 0$, and $p = 0.036$; for 0.4°, 0.8°, 1.4°, 2°, 3°, and 6°, respectively, Monte Carlo simulated likelihood test).

We next tested whether size also affected the time duration over which the bright and dark afterimages were perceived. Overall, we found significant effects of stimulus polarity and size on the perceived duration of afterimages (Fig. 2*D*, bottom, $F = 76.19$, $p = 5.20 \times 10^{-5}$ and $F = 27.79$, $p = 2.90 \times 10^{-11}$, respectively; $N = 8$ subjects), as well as a significant interaction between these two factors ($F = 23.88$, $p = 2.23 \times 10^{-10}$; $N = 8$ subjects; two-way repeated-measures ANOVA). Tukey's *post hoc* analyses

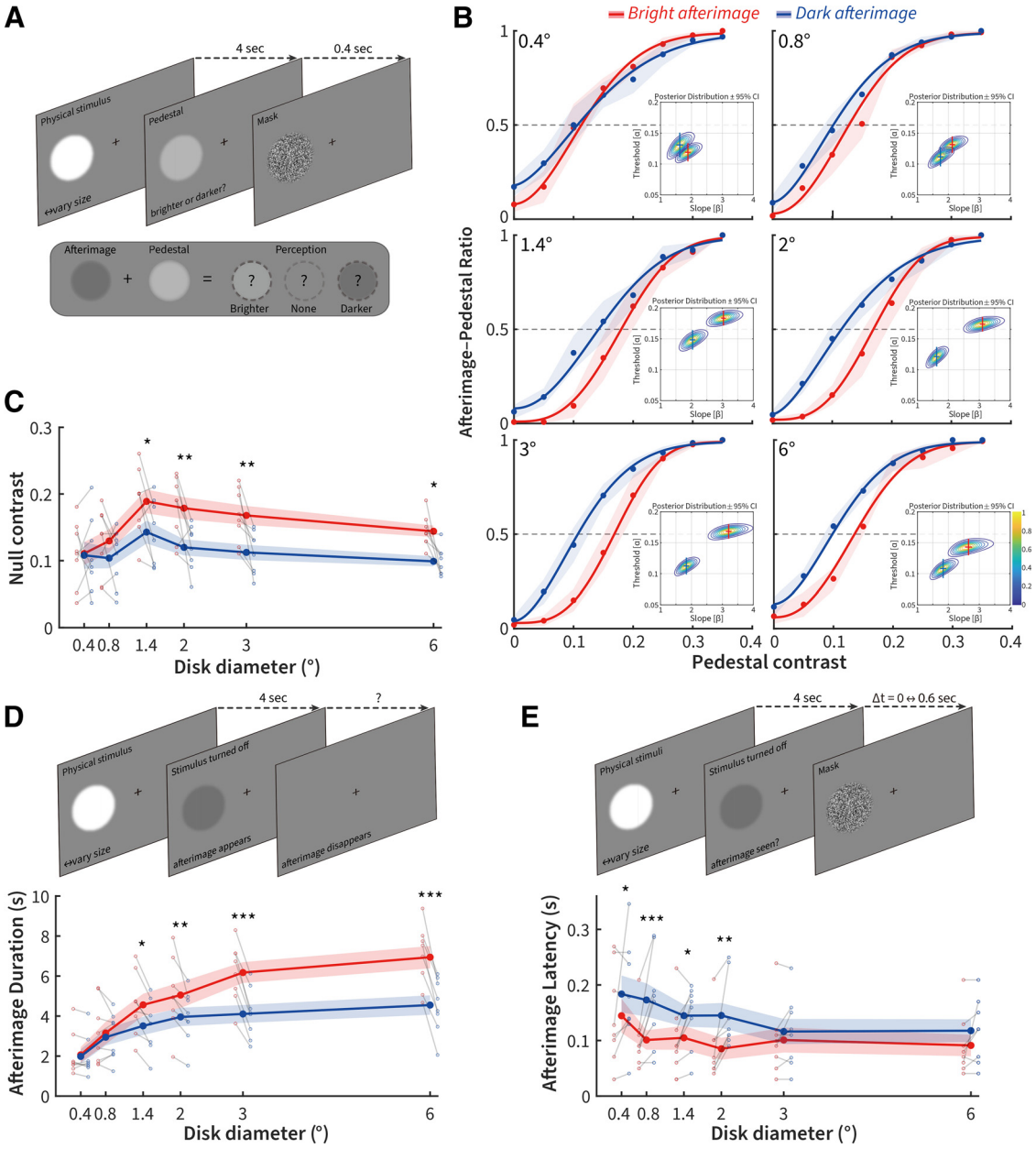

Figure 2. Stimulus size affects perceived asymmetries between dark and bright afterimages. ***A***, Pedestal nulling paradigm consisting of an afterimage-inducing bright or dark disk followed by a luminance pedestal for 0.4 s; subjects were asked whether the post-stimulus period before the mask was perceived as brighter, darker, or the same as the background. ***B***, Quick psychometric functions and their Bayesian posterior distributions for threshold and slope (inset, crosses indicate ±95% CI) for the pedestal contrast. ***C***, Tuning curves for the null contrast of bright and dark afterimages across size, along with individual subject grouped scatter plots at each size (gray lines connect the bright and dark points for each subject). ***D***, Top, Psychophysical paradigm for duration measurement. Bottom, Mean afterimage duration tuning curves and subject scatterplots for dark and bright stimuli. ***E***, Top, Psychophysical paradigm for latency measurement. Bottom, Mean latency tuning curves and subject scatterplots for Δt mask thresholds between bright and dark afterimages. $N = 8$ subjects. Error bars indicate ±1 SEM. $^{*}p < 0.05$. $^{**}p < 0.01$. $^{***}p < 0.001$.

showed that the perceived duration of bright afterimages was significantly greater than the duration of dark afterimages at sizes >0.8° ($p = 0.94$, $p = 0.60$, $p = 0.01$, $p = 0.0076$, $p = 5.51 \times 10^{-6}$, and $p = 5.11 \times 10^{-7}$ for 0.4°, 0.8°, 1.4°, 2°, 3°, and 6°, respectively; $N = 8$ subjects).

We finally measured whether size had an impact on perceptual latency for dark versus bright stimulus driven afterimages. Our paradigm attempted to determine whether there was any difference in the perception of bright and dark afterimages to a backward mask of varying delay (Fig. 2*E*, top). Subjects had to report whether any afterimage was perceived before a dynamic white noise mask turned on. Using a two-way repeated-measures ANOVA, we found a significant effect of stimulus polarity, size, and their interaction on the perceived latency of the afterimage (polarity: $F = 10.07$, $p = 0.016$; size: $F = 6.96$, $p = 1.32 \times 10^{-4}$; interaction: $F = 2.90$, $p = 0.027$; $N = 8$ subjects). Tukey's *post hoc* tests revealed that bright afterimages appeared significantly earlier than dark afterimages at sizes <3° ($p = 0.029$, $p = 1.73 \times 10^{-4}$, $p = 0.026$, $p = 0.0013$, $p = 0.38$, and $p = 0.13$ for 0.4°, 0.8°, 1.4°, 2°, 3°, and 6°, respectively; $N = 8$ subjects).

Collectively, our psychophysical results demonstrate that asymmetries in the strength and duration of bright versus dark afterimages emerge for stimuli >0.8°, whereas latency differences

were only apparent at sizes <3°. This demonstrates that size influences the strength, duration, and latency of the asymmetry between dark and bright afterimages, although the relationship between stimulus size and latency is reversed compared with the strength and duration of the afterimage perception.

The effects of size on stimulus–response asymmetries for ON versus OFF cells

Responses were quantitatively measured for 168 cells within dLGN A and A1 laminae in 18 adult cats. Ten sizes of dark and bright disk stimuli with the same contrast against an identical mid-level background were presented within the RF of each dLGN cell examined. The recorded RF locations had a mean eccentricity of 4.3° from the area centralis, and the population comprised 93 ON-center cells (73 X and 20 Y cells) and 75 OFF-center cells (52 X and 23 Y cells). The responses of putative RGCs recorded using S-potentials comprised 26 ON- and 22 OFF-center cells. There was no significant difference in the RF size measured using white noise between ON and OFF cells (93 ON cells: 2.01 ± 0.12°, 75 OFF cells: 2.34 ± 0.17°; $p = 0.13$, Wilcoxon rank-sum). There was also no such difference in X cells (73 ON-X cells: 2.02 ± 0.15°, 52 OFF-X cells: 2.18 ± 0.20°; $p = 0.50$, Wilcoxon rank-sum). ON-Y cells exhibited smaller averaged RF size than OFF-Y cells, although this was not statistically significant (20 ON-Y cells: 1.97 ± 0.24°, 23 OFF-Y cells: 2.70 ± 0.33°; $p = 0.13$; Wilcoxon rank-sum). We took advantage of the ability to record S-potentials from putative RGCs by carefully spike-sorting the dLGN recordings (Li et al., 2017). There was no significant difference of RF size measured with white noise between ON- and OFF-RGCs (26 ON-RGCs: 1.88 ± 0.20°, 22 OFF-RGCs: 2.19 ± 0.26°; $p = 0.57$, Wilcoxon rank-sum).

Size tuning is a standard method to measure RF structure and center-surround antagonism in visual neurons. To serve as a comparative baseline to our post-stimulus measurements, we first tested size-dependent subcortical ON and OFF cell stimulus responses to same-polarity bright or dark disks. Figure 3*A* plots the PSTHs of representative OFF- and ON-center cells in response to dark and bright disks with a diameter of 2°. For a dark stimulus (Fig. 3*A*, left), the same-polarity OFF cell response was facilitated at stimulus onset, whereas the opposite-polarity ON cell response was suppressed during stimulus onset but facilitated at its offset. Conversely, for a bright disk (Fig. 3*A*, right), the same-polarity ON cell response was facilitated at stimulus onset, whereas the opposite-polarity OFF cell response was suppressed during stimulus onset but facilitated at its offset.

Figure 3*B* shows surface plots of population responses to a series of same-polarity disk stimuli of different diameters (*y* axis) over time (*x* axis) after stimulus onset and offset in ON and OFF cells. We calculated the stimulus responses to same-polarity stimuli across all sizes by averaging the firing rate of each cell during the first 300 ms after stimulus onset. We found that the responses were stronger for ON than OFF cells at small sizes and for OFF than ON cells at large sizes (Fig. 3*C*, left), demonstrating size-dependent ON and OFF asymmetries for same-polarity stimuli in dLGN cells. Separating out our population into X and Y cells, X cells showed similar size-dependent asymmetries as described above for the overall population, with X-ON cells responding more strongly than X-OFF cells at small sizes, whereas this difference disappeared at larger sizes (Fig. 3*C*, middle). For Y cells, OFF cells showed significantly stronger responses than ON cells at the largest size, but no statistical difference at smaller sizes (Fig. 3*C*, right).

Because the ON and OFF channels originate in the retina, we next investigated whether size-dependent asymmetries could be observed between ON- and OFF-RGCs. We found no statistical difference for individual sizes between ON- and OFF-RGCs (Fig. 3*D*); however, the data trend was consistent with dLGN, and the combined 0.2° to 2° responses were larger for ON- than OFF-RGCs ($p = 0.020$, Wilcoxon rank-sum test). In summary, we show size-dependent stimulus–response asymmetries between ON and OFF cells to the onset of same-polarity stimuli, with ON cells exhibiting stronger responses at and below its optimal response size, but weaker responses at larger stimulus sizes compared with OFF cells.

Smaller RF center and stronger surround suppression for ON cells to bright stimulus onset than OFF cells to dark stimulus onset

Tuning for stimulus size depends on center-surround antagonism in the RF. The size tuning differences of dLGN ON and OFF cells to the onset of same-polarity stimuli strongly suggest a difference in the degree of center-surround antagonism between ON and OFF cells. To confirm this, we calculated the optimal size (i.e., the size that drives the maximal response) and suppression index (1 − plateau response/optimal response) for ON and OFF cells. We found that ON cells had a smaller optimal size (Fig. 3*E*, left, 93 ON cells, 75 OFF cells: 1.47 ± 0.12° vs 2.51 ± 0.22°, $p = 1.60 \times 10^{-4}$; Wilcoxon rank-sum) and a higher suppression index (Fig. 3*F*, left, 93 ON cells, 75 OFF cells: 0.85 ± 0.033 vs 0.67 ± 0.041, $p = 9.04 \times 10^{-5}$; Wilcoxon rank-sum) to the onset of bright stimuli than OFF cells to the onset of dark stimuli, consistent with the finding in macaque V1 population activity that large bright stimuli evoke stronger cortical inhibition than equally large dark stimuli (Xing et al., 2014). The same method was also used to quantify the RF properties for X and Y cells, respectively. We found that this pattern of differences in optimal size and suppression index between ON and OFF cells was seen in both X and Y cells (Fig. 3*E*,*F*, left, 73 ON-X vs 52 OFF-X: 1.45 ± 0.13° vs 2.16 ± 0.25°, $p = 0.012$ for optimal size; 0.84 ± 0.036 vs 0.73 ± 0.052, $p = 0.017$ for suppression index; 20 ON-Y vs 23 OFF-Y: 1.54 ± 0.27° vs 3.16 ± 0.44°, $p = 0.010$ for optimal size; 0.91 ± 0.078 vs 0.56 ± 0.061, $p = 0.0020$ for suppression index; Wilcoxon rank-sum). The RF size measured with bright disk stimuli was smaller than that measured with white noise in ON cells for all cells, for X cells, but not for Y cells (93 ON cells: $p = 3.51 \times 10^{-8}$, 73 ON-X cells: $p = 7.59 \times 10^{-8}$, and 20 ON-Y cells: $p = 0.076$, respectively, Wilcoxon signed-rank). There was no significant difference in OFF cells for all cells, X cells, and Y cells (75 OFF cells: $p = 0.23$, 52 OFF-X cells: $p = 0.051$, and 23 OFF-X cells: $p = 0.55$, respectively, Wilcoxon signed-rank).

We also calculated the optimal size and suppression index for S-potentials, finding that ON-RGCs had smaller optimal sizes than OFF-RGCs (Fig. 3*E*, right, 26 ON-RGCs, 22 OFF-RGCs: 1.95 ± 0.20° vs 3.49 ± 0.35°, $p = 1.3 \times 10^{-3}$; Wilcoxon rank-sum), but there was no significant difference in suppression index (Fig. 3*F*, right, 26 ON-RGCs, 22 OFF-RGCs: 0.27 ± 0.022 vs 0.22 ± 0.034, $p = 0.058$; Wilcoxon rank-sum). We also compared the optimal size with the RF size estimated using white noise. For ON-RGCs, there was no significant difference (26 ON-RGCs: $p = 0.37$; Wilcoxon signed-rank), and for OFF-RGCs, RF size measured with white noise were smaller (22 OFF-RGCs: $p = 0.011$; Wilcoxon signed-rank).

Comparing optimal size and suppression index between dLGN and retina for ON and OFF cells, we found that both ON and OFF cells in dLGN showed smaller optimal sizes and a

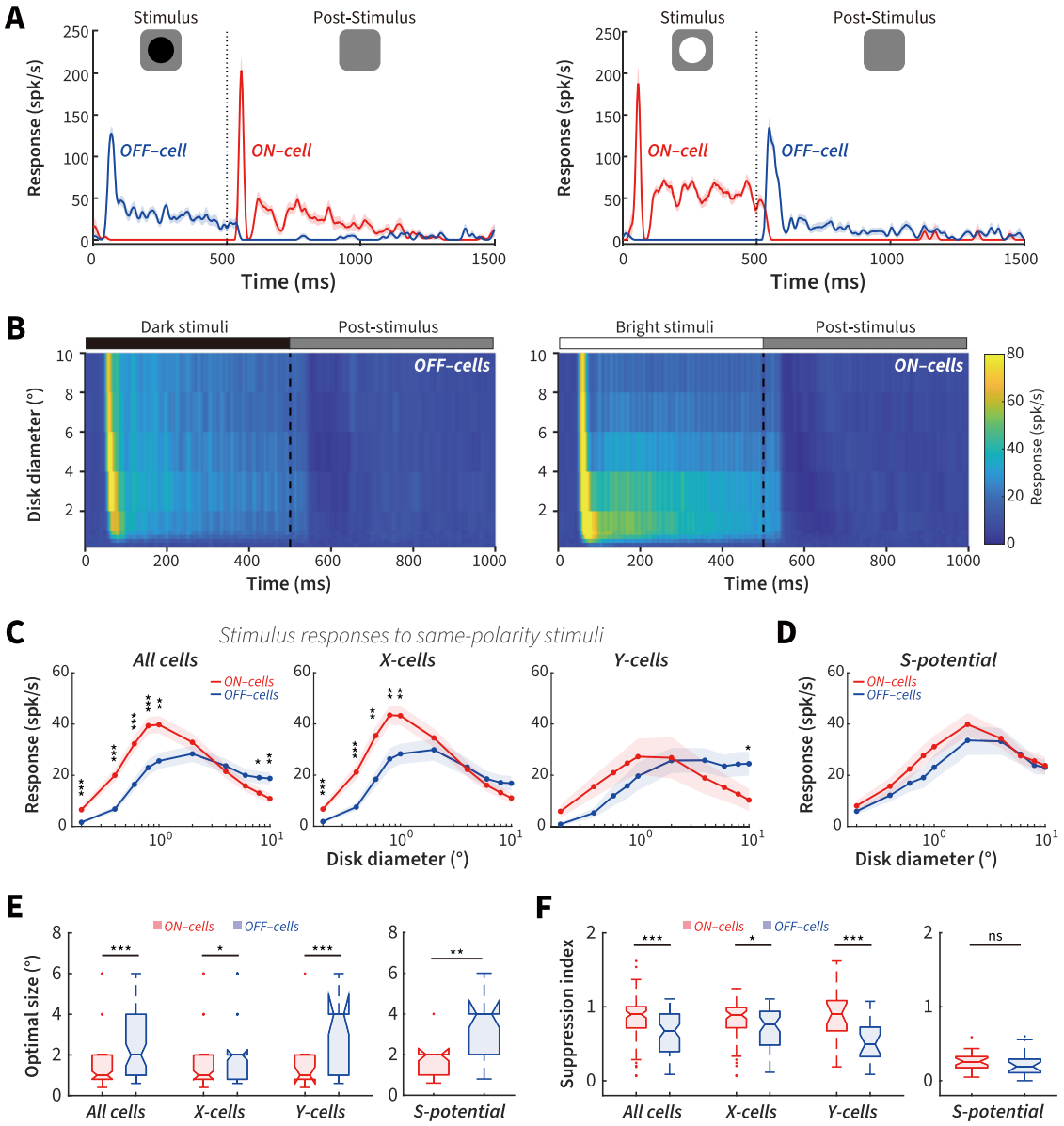

Figure 3. Same-polarity stimulus onset: pronounced differences of size tuning between ON and OFF cells. ***A***, Example ON and OFF cell responses to a 2° dark (left) and bright (right) disk stimulus onset and offset. Blue represents OFF. Red represents ON. spk/s, Spikes per second. ***B***, Color-map images of response (*z* axis) to a series of same-polarity stimuli of different diameters (*y* axis) at different times (*x* axis) after stimulus onset and offset for OFF (left) and ON cells (right). ***C***, Response plotted as a function of disk diameter for dLGN ON cells to bright stimulus onset and OFF cells to dark stimulus onset for all cells (left), X cells (middle), and Y cells (right). ***D***, Size tuning of ON-RGCs to bright stimulus onset and OFF-RGCs to dark stimulus onset. ***E***, Average optimal size of stimulus responses to same-polarity stimuli for dLGN ON and OFF cells (left) and RGCs (right). ***F***, Average suppression index of stimulus responses to same-polarity stimuli for dLGN ON and OFF cells (left) and RGCs (right). dLGN ON cells: $N = 93$ (X-ON, $N = 73$; Y-ON, $N = 20$); dLGN OFF cells: $N = 75$ (X-OFF, $N = 52$; Y-OFF, $N = 23$); ON-RGCs, $N = 26$; OFF-RGCs, $N = 22$. The PSTHs were calculated with a 1 ms bin and smoothed using a moving average Gaussian filter $\sigma = 21$ ms. *$p < 0.05$. **$p < 0.01$. ***$p < 0.001$. ns, Not significant ($p > 0.05$).

higher suppression index than RGCs (93 dLGN ON cells vs 26 ON-RGCs: optimal size $p = 0.0090$, suppression index $p = 4.23 \times 10^{-12}$; 75 dLGN OFF cells vs 22 OFF-RGCs: optimal size $p = 0.014$, suppression index $p = 2.00 \times 10^{-8}$; Wilcoxon rank-sum). The results suggest that center-surround antagonism increases in the dLGN, consistent with previous studies (Hubel and Wiesel, 1961; Cleland and Lee, 1985; Ruksenas et al., 2000).

In summary, these results demonstrate distinctly different center-surround antagonistic RF properties of ON and OFF cells to the onset of same-polarity stimuli, with ON cells showing smaller RF center and stronger surround suppression than OFF cells. This difference was more prominent in the dLGN than in the retinal afferents.

The effects of size on post-stimulus response asymmetry for ON versus OFF cells

The results above demonstrate the presence of size-dependent response asymmetries between ON and OFF cells to same-polarity stimulus onset. Negative afterimages, however, are dependent on the post-stimulus responses to opposite-polarity stimuli, so we performed the same analysis to determine whether the post-stimulus response asymmetries between ON and OFF cells to opposite-polarity stimuli were stimulus size-dependent. Post-stimulus responses (Fig. 4*A*) were calculated by averaging the firing rate of each cell during the first 300 ms after the opposite-polarity stimuli were removed from the screen (compare Fig. 3*A*).

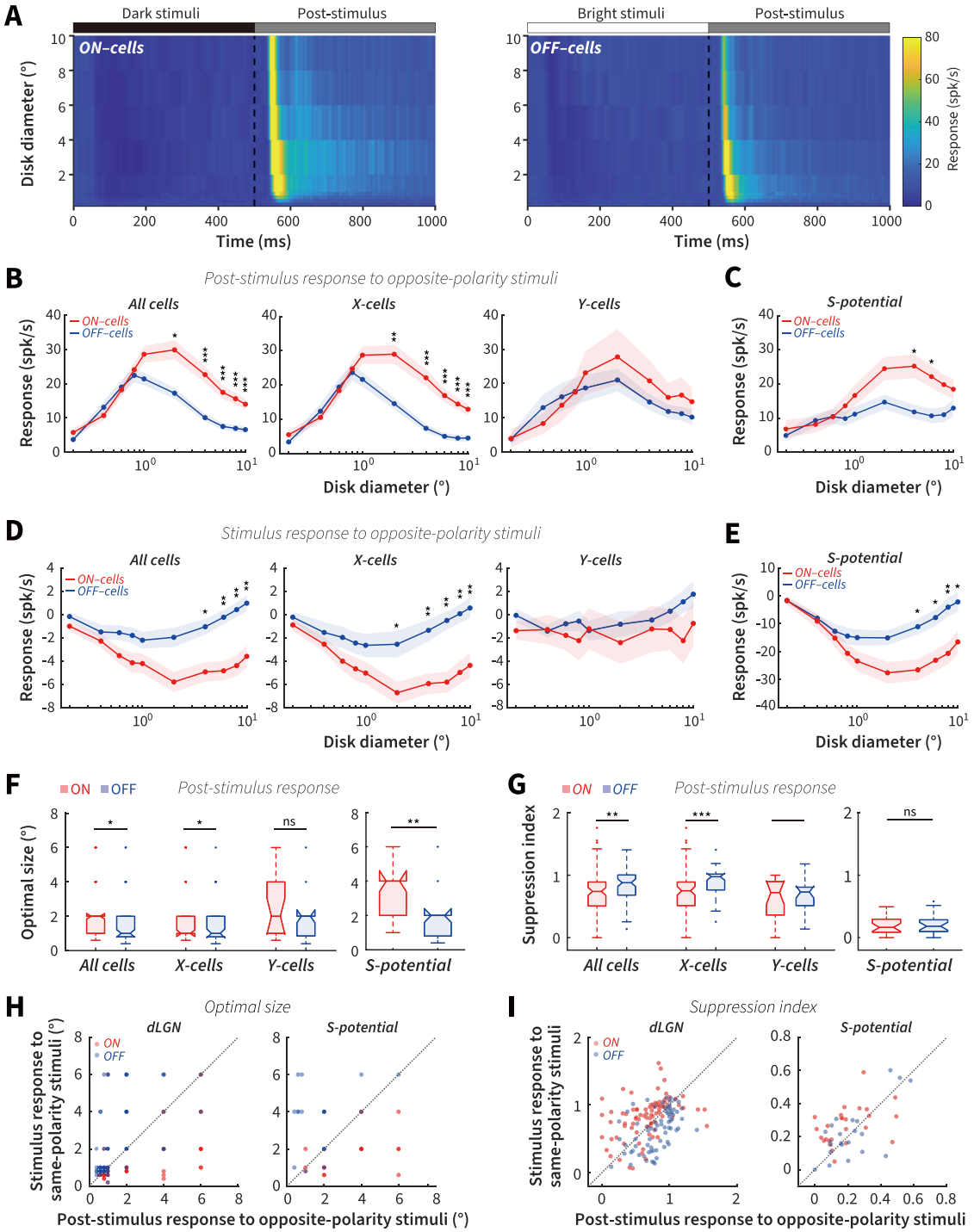

Figure 4. Stronger post-stimulus responses for ON than OFF cells to opposite-polarity stimuli at large sizes. ***A***, Color-map images of response (*z* axis) to a series of opposite-polarity stimuli of different diameters (*y* axis) at different times (*x* axis) after stimuli onset and offset in ON (left) and OFF cells (right), respectively. ***B***, Size tuning of dLGN ON cells to the offset of dark stimuli and OFF cells to the offset of bright stimuli for all cells (left), X cells (middle), and Y cells (right). ***C***, Size tuning of post-stimulus response for ON- and OFF-RGCs. ***D***, Size tuning of dLGN ON cells to the onset of dark stimuli and OFF cells to the onset of bright stimuli for all cells (left), X cells (middle), and Y cells (right). ***E***, Size tuning of stimulus response to opposite-polarity stimuli for RGCs. ***F***, Average optimal size of post-stimulus responses to opposite-polarity stimuli for dLGN cells (left) and RGCs (right). ***G***, Average suppression index of post-stimulus responses to opposite-polarity stimuli for dLGN cells (left) and RGCs (right). ***H***, Optimal size of stimulus response to same-polarity stimuli plotted against the optimal size of post-stimulus response to opposite-polarity stimuli for dLGN cells (left) and RGCs (right). ***I***, Suppression index of stimulus response to same-polarity stimuli plotted against suppression index of post-stimulus response to opposite-polarity stimuli for dLGN cells (left) and RGCs (right). $*p < 0.05$. $**p < 0.01$. $***p < 0.001$. ns, Not significant ($p > 0.05$).

Interestingly, we observed distinct size-dependent response asymmetries between ON and OFF cells to the offset of opposite-polarity stimuli compared with the onset of same-polarity stimuli. We found stronger post-stimulus responses in ON cells than OFF cells at larger sizes >1°, but no significant difference <1° (including 1°, Fig. 4*B*, left). These size-dependent asymmetries were mainly contributed by X cells but not Y cells (Fig. 4*B*, middle and right). Moreover, we found similar size-dependent post-

stimulus response asymmetries between ON- and OFF-RGCs (Fig. 4*C*).

Usually, stronger suppression from a stimulus triggers a higher postinhibitory rebound (Zaghloul et al., 2003; Wang et al., 2016); in our case, the rebound responses follow suppression induced by opposite-polarity stimuli (Fig. 4*A*). We hypothesized that the stronger ON cell post-stimulus response strength at larger sizes should be correlated with greater stimulus-dependent suppression. To estimate this relationship, we subtracted the inhibitory period firing rate during the onset of opposite-polarity stimuli from the spontaneous firing rate before stimulus presentation. We found that ON cells had significantly stronger suppression to dark stimulus onset than OFF cells to bright stimulus onset at larger, but not at smaller sizes in both dLGN X cells and RGCs (Fig. 4*D*,*E*). This resulted in a significant negative correlation between the ON − OFF difference in post-stimulus response strength and stimulus-driven suppression with size ($R = -0.75$, $p = 0.018$; Spearman correlation), supporting our prediction.

Together, these electrophysiological results demonstrate that stimulus size consistently modulates the asymmetries of post-stimulus responses to opposite-polarity stimuli between subcortical ON and OFF cells, consistent with our psychophysical findings that human observers see stronger bright afterimages than dark afterimages at larger stimulus sizes only.

Smaller RF center and stronger surround suppression for OFF cells to bright stimuli than ON cells to dark stimuli

We hypothesized that the stronger post-stimulus responses of ON versus OFF cells to opposite-polarity stimuli at larger sizes are because OFF cells exhibit stronger center-surround antagonism. Our analysis of the optimal size and suppression index supports this hypothesis. OFF cells showed a smaller optimal size and a higher suppression index than ON cells (Fig. 4*F*,*G*, left, 93 ON cells vs 75 OFF cells: 2.12 ± 0.17° vs 1.57 ± 0.14°, $p = 0.013$ for optimal size; 0.70 ± 0.035 vs 0.82 ± 0.030, $p = 0.0020$ for suppression index; Wilcoxon rank-sum). These measurements were opposite to those for stimulus response to same-polarity stimuli, where ON cells had smaller optimal sizes and higher suppression index than OFF cells (Fig. 3). Moreover, we found that X cells showed similar differences in optimal sizes and suppression index (Fig. 4*F*,*G*, left, 73 ON-X vs 52 OFF-X: 2.03 ± 0.19° vs 1.56 ± 0.17°, $p = 0.03$ for optimal size; 0.73 ± 0.039 vs 0.88 ± 0.034, $p = 4.15 \times 10^{-4}$ for suppression index; Wilcoxon rank-sum), but not Y cells (Fig. 4*F*,*G*, left, 20 ON-Y vs 23 OFF-Y: 2.45 ± 0.42° vs 1.61 ± 0.24°, $p = 0.12$ for optimal size; 0.61 ± 0.074 vs 0.71 ± 0.050, $p = 0.46$ for suppression index; Wilcoxon rank-sum). There was no significant difference of RF size measured with white noise compared with that measured with dark stimuli offset in ON cells for all cells, X cells, and Y cells (93 ON cells: $p = 0.16$, 73 ON-X cells: $p = 0.059$, and 20 ON-Y cells: $p = 0.68$, respectively, Wilcoxon signed-rank), whereas the RF size measured with bright disk stimuli offset was smaller than that measured with white noise in OFF cells for all cells, X cells, and Y cells (75 OFF cells: $p = 6.03 \times 10^{-8}$, 52 OFF-X cells: $p = 3.88 \times 10^{-6}$, and 23 OFF-Y cells: $p = 0.0032$, respectively; Wilcoxon signed-rank). There results suggest that the RF size measured with white noise is very similar with that measured with dark stimuli (onset or offset), but larger than that measured with bright stimuli (onset or offset) for both ON and OFF cells.

For S-potentials, OFF-RGCs also showed smaller optimal sizes than ON-RGCs to opposite-polarity stimuli offset (Fig. 4*F*, right, 26 ON-RGCs vs 22 OFF-RGCs: 3.35 ± 0.31° vs 1.87 ± 0.28°, $p = 1.2 \times 10^{-3}$; Wilcoxon rank-sum), but there was no significant difference in the suppression index (Fig. 4*G*, right, 26 ON-RGCs vs 22 OFF-RGCs: 0.19 ± 0.037 vs 0.22 ± 0.032, $p = 0.52$; Wilcoxon rank-sum). For ON-RGCs, RF size measured with white noise was smaller than that measured with dark stimulus offset (26 ON-RGCs: $p = 0.0020$; Wilcoxon signed-rank). For OFF-RGCs, RF size measured with white noise showed no difference with that measured with bright stimulus offset (22 OFF-RGCs: $p = 0.35$; Wilcoxon signed-rank).

Comparing optimal size and suppression index between dLGN and RGCs, we found that dLGN ON cells showed smaller optimal size and a higher suppression index than ON-RGCs (93 dLGN ON cells vs 26 ON-RGCs: $p = 1.91 \times 10^{-4}$ and $p = 1.72 \times 10^{-10}$, respectively; Wilcoxon rank-sum), and there was no significant difference in the optimal size but a significantly higher suppression index for dLGN OFF cells than OFF-RGCs (75 dLGN OFF cells vs 22 OFF-RGCs: $p = 0.35$ and $p = 3.80 \times 10^{-11}$, respectively; Wilcoxon rank-sum). These results suggested that the increase of center-surround antagonism for stimulus responses in the dLGN is also reflected in the post-stimulus responses.

We further compared optimal size and suppression index for ON and OFF cells between stimulus responses to same-polarity stimuli and post-stimulus responses to opposite-polarity stimuli. We confirmed that ON cells showed a smaller optimal size and a higher suppression index to bright stimulus onset than to dark stimulus offset (Fig. 4*H*,*I*, left, $p = 2.09 \times 10^{-7}$ and $p = 7.30 \times 10^{-6}$, respectively, $N = 93$; Wilcoxon signed-rank), and OFF cells showed smaller optimal size and a higher suppression index to bright stimulus offset than to dark stimulus onset (Fig. 4*H*,*I*, left, $p = 1.13 \times 10^{-6}$ and $p = 4.13 \times 10^{-6}$, respectively, $N = 75$; Wilcoxon signed-rank). There were similar differences in optimal size between stimulus and post-stimulus responses in ON- and OFF-RGCs (Fig. 4*H*, right, 26 ON-RGCs, $p = 4.60 \times 10^{-4}$ 22 OFF-RGCs, $p = 3.66 \times 10^{-4}$; Wilcoxon signed-rank). For the suppression index, ON-RGC cells, but not OFF-RGC cells, showed differences similar to the dLGN relay cells (Fig. 4*I*, right, 26 ON-RGCs, $p = 0.0068$; 22 OFF-RGCs, $p = 0.6143$; Wilcoxon signed-rank).

Together, these results demonstrate that the bright disk post-stimulus responses of opposite-polarity subcortical OFF cells are tuned to a smaller optimal size and stronger surround suppression. In contrast, the dark disk post-stimulus responses of opposite-polarity ON cells showed bigger RF centers and weaker surround suppression. This resulted in a stronger post-stimulus response for ON cells to dark stimuli than OFF cells to bright stimuli at larger sizes. This neural response difference parallels the asymmetry we observed in the perceived strength of bright and dark afterimages (Fig. 2*A*–*C*).

Size-dependent asymmetries in the temporal response properties of ON and OFF cells

Many early visual neurons respond to light with transient/sustained temporal response properties, which depend, in part, on the relative levels of excitatory and inhibitory input (Ikeda and Wright, 1972; Awatramani and Slaughter, 2000; Margolis and Detwiler, 2007). Here we examined the temporal response properties measured using a sustained index for ON and OFF cells to the onset of same-polarity stimuli and the offset of opposite-polarity stimuli. The sustained index was calculated as the ratio of the mean response of the first 300 ms after stimulus onset or offset to the peak response of the PSTH with 1 ms bins. A larger sustained index indicates a less transient response. For the stimulus response to same-polarity stimuli, the sustained index was larger for ON than OFF cells at small sizes, and for OFF than

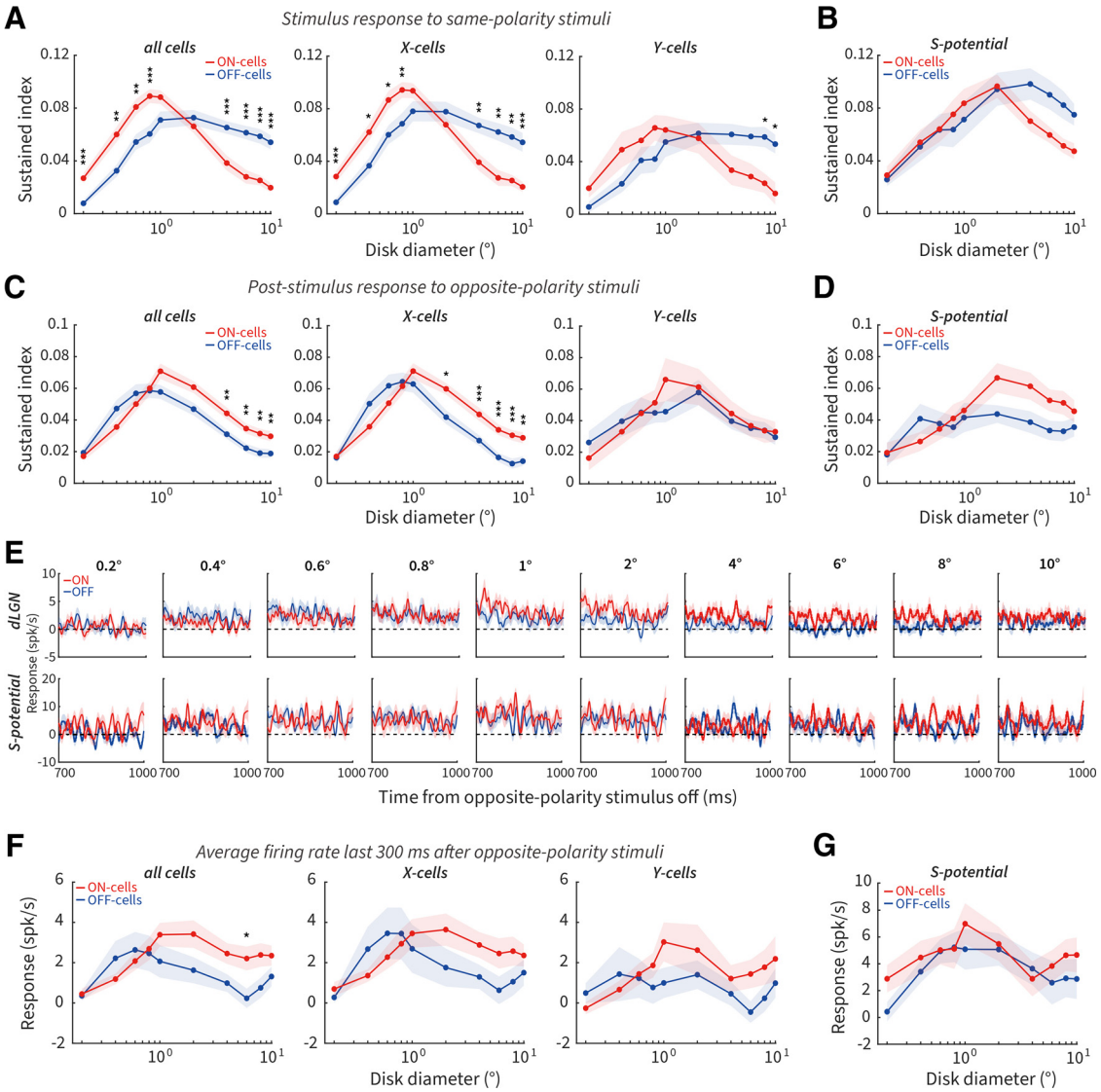

Figure 5. Pronounced differences of sustained index between ON and OFF cells. ***A***, Size tuning of sustained index for ON and OFF cells to the onset of same-polarity stimuli for all cells (left, 93 ON, 75 OFF), X cells (middle, 73 ON, 52 OFF), and Y cells (right, 20 ON, 23 OFF) in dLGN. ***B***, Size tuning of the sustained index for ON- ($N = 26$) and OFF-RGCs ($N = 22$) to the onset of same-polarity stimuli. ***C***, ***D***, Same as in ***A***, ***B***, but to the offset of opposite-polarity stimuli. ***E***, Population PSTHs for dLGN (top) and RGCs (bottom) from 700 to 1000 ms after the offset of opposite-polarity stimuli of different diameters. Dotted line indicates baseline firing. ***F***, Size tuning of the final 300 ms of the response for all cells (left, 67 ON, 57 OFF), X cells (middle, 49 ON, 36 OFF), and Y cells (right, 18 ON, 21 OFF) in the dLGN. ***G***, Size tuning of the final 300 ms of the response for ON- ($N = 21$) and OFF-RGCs ($N = 15$). $^*p < 0.05$. $^{**}p < 0.01$. $^{***}p < 0.001$.

ON cells at large sizes (Fig. 5*A*, left). We found similar size-dependent asymmetries of the sustained index between X-ON cells and X-OFF cells as described above (Fig. 5*A*, middle). Y-OFF cells showed a larger sustained index than Y-ON cells at large sizes (Fig. 5*A*, right). We also performed the sustained-index analysis on the S-potential responses. Consistent with dLGN cells, we saw a trend for a larger (although not significantly so after multiple comparisons correction) sustained index for OFF- than ON-RGCs at larger sizes only (Fig. 5*B*).

For the post-stimulus responses to opposite-polarity stimuli, the sustained index was larger for ON than OFF cells at large sizes, and there was no difference at small sizes (Fig. 5*C*, left). This size-dependent asymmetry in the sustained index was mainly contributed by X cells (Fig. 5*C*, middle and right). There was no significant difference of sustained index between ON- and OFF-RGCs across size (Fig. 5*D*).

Stimulus presentations of differing lengths cause different levels of neural adaptation across the visual system. Tested with one stimulus size and long stimulus presentation times, our previously published results demonstrated that longer stimulus presentation times resulted in a larger perceived duration for dark than bright afterimages, paralleled by longer post-stimulus elevations of firing rate for ON versus OFF cells (Li et al., 2017, their Figs. 2*E* and 4). Although the presentation times of our stimuli here were shorter, we wished to investigate the impact of stimulus size on elevated firing rates, we calculated the average firing rates from 700 to 1000 ms after opposite-polarity stimuli offset. Population PSTHs of this final 300 ms of the response for each size are shown in Figure 5*E*. The averaged firing rates were slightly higher for dLGN ON versus OFF cells at sizes $\geq 1°$ (Fig. 5*F*, left, although only 6° was significant after multiple comparisons correction), consistent with our psychophysical observation that dark stimuli produced negative afterimages with longer perceptual durations at larger ($>0.8°$), but not at smaller sizes. X and Y cells showed a similar trend (Fig. 5*F*, middle and right); however, this difference was not observed between ON- and OFF-RGCs (Fig. 5*G*).

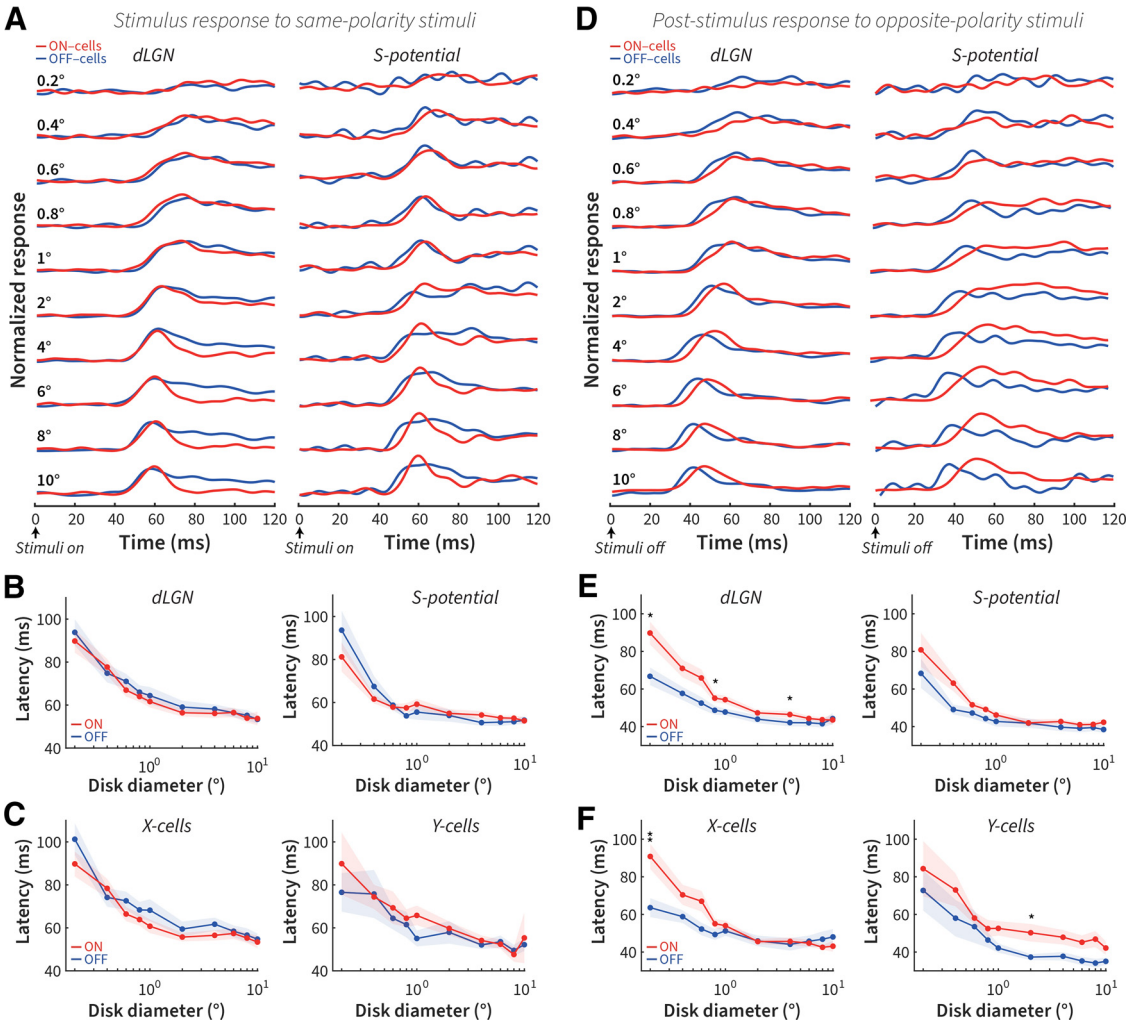

Figure 6. Post-stimulus responses are faster for OFF cells than for ON cells. ***A***, Normalized PSTH of the first 120 ms for dLGN ON and OFF cells (left) and RGCs (right) to the onset of same-polarity stimuli. ***B***, Size tuning of response latencies for dLGN ON and OFF cells (left, 86 ON, 62 OFF) and RGCs (right, 25 ON, 21 OFF) to the onset of same-polarity stimuli. ***C***, Size tuning of response latencies for X (left, 71 ON, 46 OFF) and Y cells (right, 15 ON, 16 OFF). ***D***, Same as in ***A***, but for opposite-polarity stimulus offset. ***E***, Same as in ***B***, but for opposite-polarity stimulus offset. ***F***, Same as in ***C***, but for opposite-polarity stimulus offset. $^{*}p < 0.05$. $^{**}p < 0.01$.

We conclude that stimulus size influences transient/sustained response properties for same-polarity stimulus onset and opposite-polarity stimulus offset responses in ON and OFF cells. ON cells exhibited more transient responses for same-polarity stimuli and more sustained responses for opposite-polarity stimuli at larger sizes compared with OFF cells. In addition, only larger stimulus sizes caused an asymmetrical elevation of post-stimulus response lasting up to the 1000 ms tested in ON cells. These results are consistent with size-dependent changes in the surround suppression of ON cells (being stronger as observed in Fig. 3*F* for same-polarity onset responses and weaker as observed in Fig. 4*G* for opposite-polarity offset responses), causing weaker or stronger sustained responses (Awatramani and Slaughter, 2000; Buldyrev and Taylor, 2013).

Latency differences in the post-stimulus responses of ON and OFF cells

To compare the latency differences between ON and OFF cells, we plotted the averaged and normalized PSTHs and resultant latency estimates after same-polarity stimulus onset (Fig. 6*A–C*) and opposite-polarity stimulus offset (Fig. 6*D–F*). Overall, there is a clear inverse relationship between response latency and stimulus size. Statistically, there was no difference in the response latency between ON and OFF cells to same-polarity stimulus onset in dLGN and retina (Fig. 6*B*), and therefore no latency difference between X and Y cells (Fig. 6*C*). Jin et al. (2011) have previously shown that onset response of thalamic OFF cells is on average 4 ms faster than ON cells, whereas our previous and current study did not see this difference; some of the possible reasons are discussed in our previous paper (Li et al., 2017). For opposite-polarity post-stimulus responses, OFF cells exhibited shorter latencies than ON cells mostly for smaller sizes in dLGN (significantly so at 0.2°, 0.8°, and 4°; Fig. 6*E*, left); compare Li et al. (2017) where a significant difference was seen at 2° (we have corrected the FWER for multiple comparisons because of analyzing multiple sizes, and this more conservative estimate explains the statistical discrepancy). This trend was observed in RGCs (Fig. 6*E*, right) and both X and Y cells (Fig. 6*F*). These results demonstrate that latency differences between ON and OFF cell post-stimulus responses to opposite-polarity stimuli are inconsistent with the perceptual latency difference observed between bright and dark afterimages (Fig. 2*E*), although these latencies are quite different in time scale.

The eDOG model demonstrates spatiotemporal RF parameter differences between ON and OFF cells

The data so far suggest that size-dependent asymmetries are related to weaker surround suppression and more sustained response properties in ON cells than OFF cells at the removal of opposite-polarity stimuli. Classically, difference-of-Gaussians (DOG) models have been used to model the integration of excitatory and inhibitory interactions across changes in size (Rodieck, 1965; Sceniak et al., 2001). However, the DOG can only model spatial integration. To account for post-stimulus response changes over time we used a firing-rate network model (extended DOG, or eDOG) (Mobarhan et al., 2018) that includes both the spatial and temporal parameters of RGCs and dLGN relay cells. In the model, ON- and OFF-RGCs provide feedforward excitation and inhibition to model ON and OFF dLGN relay cells. The eDOG model is firing-rate based and generates post-stimulus rebound response after removal of visual stimulation. Mathematically, the model RF is defined by spatial and temporal impulse–response functions: RGCs includes DOG spatial and biphasic temporal functions. The output functions are integrated at the thalamic network level using a spatial Gaussian function and temporal exponential decay function by feedforward coupling kernels. Feedforward excitation and inhibition from ON- and OFF-RGCs have their own coupling kernels, enabling quantification of the differences between them.

Figure 7*A* (left) shows the averaged population responses for OFF and ON cells to same-polarity stimuli as shown in Figure 3*A*; this averaged response profile was fitted by the eDOG using gradient descent to yield model surface plots shown in Figure 7*A* (right). The parameters of this fit were then used to estimate the spatial summation profile for ON and OFF cells (without any further fitting to the data), demonstrating a close agreement between the model estimates and the averaged neural population data (Fig. 7*B*). The spatial and temporal parameters plotted in Figure 7*C–E* demonstrate a tighter center spatial response and a larger and more transient biphasic temporal response for ON cells (Ravi et al., 2018). These model results for same-polarity stimulus onsets were consistent with the smaller optimal size (Fig. 3*E*), larger suppression index (Fig. 3*F*), and more transient responses (Fig. 5*A*) for ON compared with OFF cells.

We next performed the same model fitting and analysis for the opposite-polarity stimuli (Fig. 7*F*). Again, the resultant spatial summation profiles derived from model parameters closely reflected the neural population spatial summation curves (Fig. 7*G*). We have demonstrated above that, for the responses to opposite-polarity stimuli (e.g., Figs. 4, 5*C*), tuning characteristics are largely reversed compared with the responses to same-polarity stimuli for optimal size, suppression index, and sustained index. This is recapitulated by the spatiotemporal RF of model ON and OFF cells shown in Figure 7*H-J* (compare with Fig. 7*C–E*); here it is OFF cells that exhibit a smaller spatial and larger and more transient temporal response structure.

The RF properties that encompass the preferred and nonpreferred stimuli derived from the model reinforce our conclusions from the neural results, suggesting that asymmetries between ON and OFF cells can be extrapolated from differences in RF center and surround antagonism that changes across stimulus size and polarity. Specifically, ON cells demonstrated weaker suppression, larger RF centers, and more sustained responses to opposite-polarity stimuli, parallel to the asymmetries observed in our neural and psychophysical results.

Recurrent spiking neural network model of V1

Finally, to better explain the relationship between dLGN post-stimulus response differences and the psychophysical results, we wanted to estimate the downstream effects of the thalamic activity in cortical areas. We used a recurrent spiking neural network model of V1 activity (Schwabe et al., 2006; Han et al., 2021), assuming that V1 serves as the major upstream source of the eventual perceptual responses. The firing rate of dLGN ON and OFF cells recorded in the electrophysiological experiments (Fig. 4*A*) was transformed to Poisson spike trains and used as the input of the recurrent cortical network (Fig. 8*A*). We selected 7 stimulus sizes: 0.4°, 0.6°, 0.8°, 1°, 2°, 4°, and 6°, considered to activate 2, 5, 8, 13, 50, 200, and 450 V1 neurons, respectively (the area of stimuli being proportional to the number of activated neurons). Figure 8*B* shows the post-stimulus PSTH activity of the V1 excitatory neurons across stimulus size. We calculated the average firing rate for the first 300 ms to construct a size tuning curve, and we found that the cortical ON-response is stronger than the OFF-response at larger sizes only (Fig. 8*C*; compare. Figs. 2*C*, 4*B*).

We also measured the duration of the model response, defined as the time between stimulus offset and the firing rate first dropping to <1 Hz. We found that the larger the stimulus size, the longer the neural response duration (Fig. 8*D*; compare Figs. 2*D*, 5*F*).

While it is unknown where and how spiking activity in early visual areas is transformed into a subjective perception, our model demonstrates that the subcortical post-stimulus response asymmetries can be propagated through cortical areas. The ON population exhibited stronger and longer duration post-stimulus responses at larger sizes than the OFF population. A downstream decision-making system (Najafi and Churchland, 2018) sampling such propagated activity could make perceptual choices consistent with our psychophysical results and previous studies where large-sized visual stimuli generate more persistent subjective perception (Ono and Kawahara, 2007; Rammsayer and Verner, 2014).

Discussion

Both stimulus polarity and size exert major impacts on the encoding of visual information from the earliest stages of the retina (Thoreson and Mangel, 2012) onwards. The statistical differences (more decrements than increments) present in the distribution of contrast in natural scenes (Geisler, 2008; Ratliff et al., 2010) have shaped ON and OFF channel asymmetries that are ultimately reflected in differences in our subjective perception of bright and dark negative afterimages (Li et al., 2017). These afterimages depend on stimulus presentations that drive suppression-derived rebound firing responses. Because stimulus polarity and size selectivity are so closely intertwined, we hypothesized that asymmetries in the ON and OFF post-stimulus responses and the resultant dark and bright perceptual afterimages will be positively correlated with stimulus size. We first tested whether there was any impact of stimulus size on previously identified asymmetries between dark and bright afterimages in human observers. We found that subjects exhibited a pronounced difference in the perceived strength and duration of dark and bright afterimages for stimulus diameters $>0.8°$. We further demonstrated that neural correlates for strength and duration could be found in the putative retinal afferents and dLGN relay cells in the cat. ON-RGC and dLGN cells fired more strongly to the removal of dark disks than OFF cells to the

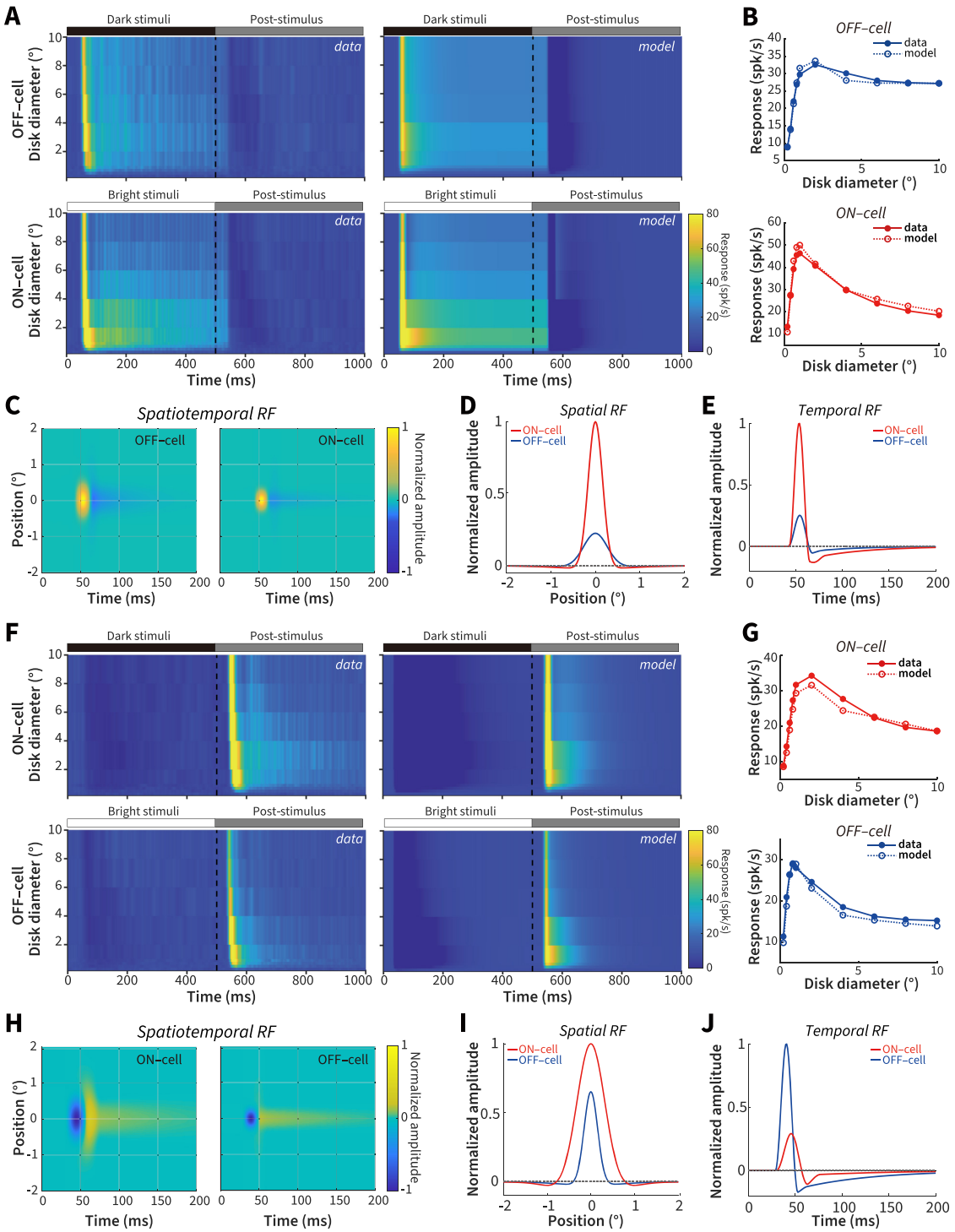

Figure 7. Spatiotemporal RF properties of dLGN ON and OFF cells. ***A***, Neural data population responses and eDOG model responses for ON and OFF cells to the onset of same-polarity stimuli. ***B***, Size tuning for the onset of same-polarity stimuli for neural data and model ON and OFF cells. ***C***, EDOG model fit spatiotemporal RF for ON and OFF cells to the onset of same-polarity stimuli. ***D***, Spatial impulse–response function for ON and OFF cells to the onset of same-polarity stimuli. ***E***, Temporal impulse–response function for ON and OFF cells to the onset of same-polarity stimuli. ***F-J***, Same as in ***A-E***, but for the response to opposite-polarity stimuli.

removal of bright disks at larger sizes >1°, but not below the optimal size defined by the spatial extent of the RF. These disk sizes are the maximum response sizes driven mainly by excitatory or disinhibitory inputs, the transition points between ascending (central excitatory/disinhibitory) and descending (surround suppression) phases in the size tuning curves of ON and OFF cells. Moreover, the post-stimulus response of ON cells in the dLGN lasts longer than the post-stimulus response of OFF cells at larger, but not smaller sizes (a result that was not observed in putative RGC afferents). Using a firing-rate based retino-geniculate model, size-dependent asymmetries were confirmed to be related with weaker surround suppression and more sustained response properties in ON cells than OFF cells to the removal of opposite-polarity stimuli. A recurrent spiking neural network model demonstrated that downstream cortical area V1 can propagate size-dependent strength and duration

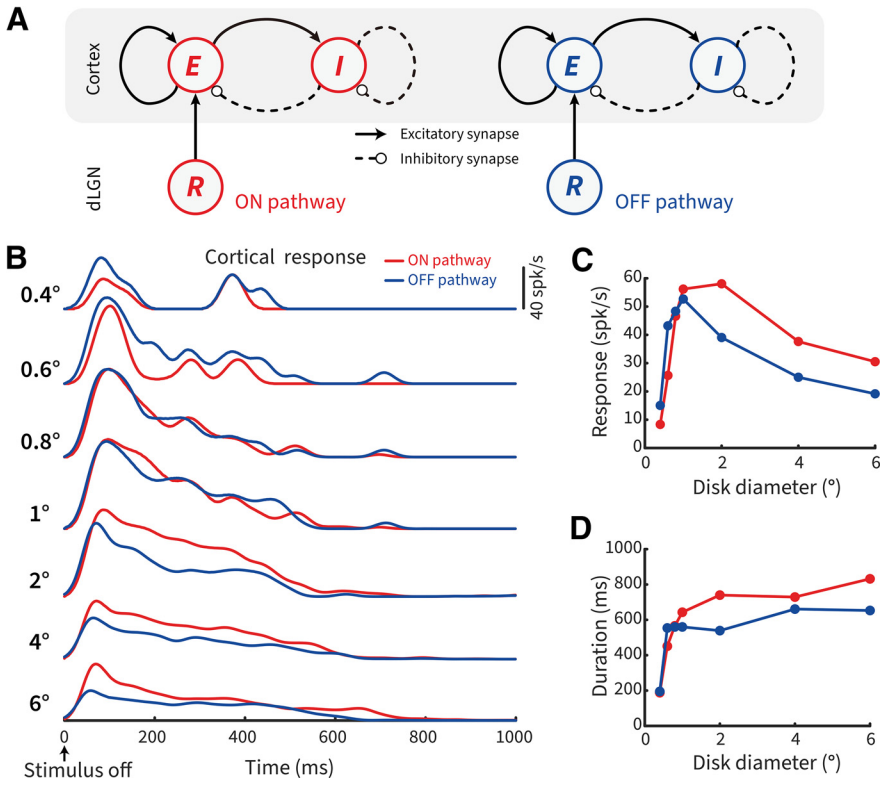

Figure 8. Recurrent spiking neural network model of V1 activity in response to LGN output. ***A***, Schematic overview of the recurrent spiking neural network model: ON and OFF dLGN relay cells (R), cortical excitatory cells (E), and cortical inhibitory cells (I) comprise the network cell types. In V1, ON and OFF populations receive input from dLGN ON and OFF cells, respectively. ***B***, PSTH post-stimulus ON (red) and OFF (blue) responses in V1 after a variable diameter stimulus was removed from view. ***C***, ON and OFF averaged firing rate size tuning curves. ***D***, ON and OFF maximum duration size tuning curves.

asymmetries between ON and OFF pathways, further supporting the subcortical origin of the differences between bright and dark negative afterimages.

Bridging the explanatory gap between sensation and neural representation

There is a wide and, as yet, unfathomed gap between the neural representations of visual stimuli and their perceptual subjective phenomenology. It is not possible to use subjective verbal report in nonverbal animals as we do for humans. Therefore, one may question whether comparing human perceptual phenomenology against animal electrophysiology is a worthwhile endeavor. Given the critical foundational nature of this question to neuroscience, it has been subject to a great deal of investigation. For example, pioneering studies by Horace Barlow (Barlow, 1972) entertained topics ranging from the quantal threshold limits of sensation (Barlow, 1956; Barlow et al., 1971) to a neural explanation of the negative motion aftereffect (Barlow and Hill, 1963). Other studies used paradigms, such as size tuning used in electrophysiological studies to compare human and nonhuman primate psychophysical and neural tuning performance (Oehler, 1985; Spillmann et al., 1987). These studies found a close match, and such behavioral measurements were termed perceptive fields, equivalent to the neural RF (Jung and Spillmann, 1970; Ransom-Hogg and Spillmann, 1980; Spillmann, 2009; Spillmann et al., 2015). Signal detection theory has been used to better estimate the relationship between perceptual psychometric and neurometric tuning functions (Parker and Newsome, 1998; Law and Gold, 2010). Recently, there has been a concerted effort in testing a wider range of visual illusions by measuring nonverbal behavior in many species of animals. Species as diverse as the fruit fly (Agrochao et al., 2020), fish (Gori et al., 2014; Y. Wu et al., 2020), reptiles (Santacà et al., 2019), cats (Bååth et al., 2014; Szenczi et al., 2019), and nonhuman primates (Subramaniyan et al., 2013; Agrillo et al., 2015; Luo et al., 2019) respond to visual illusions in a manner consistent with the way they are perceived. For example, using a perceptual nulling paradigm, we were recently able to estimate the subjective perceptual strength of a complex motion illusion in nonhuman primates (Luo et al., 2019).

We did not attempt to compensate between cat and human eccentricity differences in RF size but used the same average sizes when collecting psychophysical and electrophysiological data. At any given eccentricity, the primate visual system will afford higher spatial resolution, and we would thus expect that, if anything, we may not have seen any reduction in asymmetry in psychophysical measurements >0.8°, but that was not the case. We saw the same pattern of results >0.8° in the human observers and at ~1° in the cat, and so we believe that differences between species were not a significant issue. Another factor, which will contribute to potential differences, is the shorter stimulus presentation times (0.5 s) that we used for neural recordings compared with our psychophysical protocols (4 s). This was necessary to limit the overall data collection times required for measuring across many stimulus sizes. Longer presentation times will yield stronger and longer duration effects (Li et al., 2017), and so we believe that longer presentation times for the neural data would have only strengthened the asymmetries that we observed.

The data that we present here, looking at the effects of RF structure in early visual areas on the links between rebound responses and sensory evaluation, fit into this broader pattern aligning neural responses with perceptual phenomena. It is important to state that much of the work described above, including our own, is correlational. Much of the explanatory gap remains. We are hopeful that the novel advances in causal experimental tools that will enable cell-type, spatially and temporally precise perturbations during behavior driven by visual perception (J. Wu et al., 2020), can close this gap in the near future.

Elucidating RF mechanisms sensitive to size

Stimulus size drives an interaction between central and surrounding regions of visual space that has been conceived in terms of a "classical" RF (Hartline, 1940; Barlow, 1953; Kuffler, 1953; Hubel and Wiesel, 1962; Spillmann, 2014), in which visual stimulation elicits direct neural firing (ON, OFF, or mixed sign); and an "extended" modulatory surrounding area (extra-classical RF) (Allman et al., 1985; Spillmann et al., 2015) that cannot itself drive the cell to fire. In the dLGN, one or a few retinal afferents provide the driving input to relay cells (Mastronarde, 1987a,b;

Usrey et al., 1999; Nolt et al., 2004); therefore, the core afferent-driven RF is broadly similar between RGCs and relay cells. There are nevertheless substantial additional inputs into the dLGN, and the majority of synapses are not from the retina but from the visual cortex, the TRN, and brainstem; such inputs can contain very distinct spatial and functional specificity (Erişir et al., 1997; Liu and Jones, 1999; Murphy et al., 1999, 2000; Van Horn et al., 2000; Budd, 2004; Angelucci and Sainsbury, 2006; Briggs and Usrey, 2009). The inputs from the TRN contact both relay cells and inhibitory interneurons (Uhlrich et al., 1991, 2003; Uhlrich and Cucchiaro, 1992) originate from cells with larger RFs than relay cells (Sillito and Jones, 2008), and have the power to strongly modulate responses of relay cells to retinal input (Funke and Eysel, 1998). Inhibitory interneurons themselves are involved in both the X stream, where they form unique synaptic glomeruli (triadic synapses) for feedforward inhibitory-locked transmission through the X pathway (Sherman and Guillery, 2002; Sherman, 2004), and more heterogeneous connectivity for the Y stream (Datskovskaia et al., 2001). Inhibitory interneurons exhibit both axo-dendritic and dendro-dendritic connections between multiple cell types (Hamos et al., 1985; Montero, 1986, 1987), enabling them to process inputs dynamically and contextually across relay cells and other interneurons with a greater spatial scale than the relay cells alone (Acuna-Goycolea et al., 2008; Lindström and Wróbel, 2011; Crandall and Cox, 2012).

Consistent with these known differences, we found a larger optimal diameter and weaker surround suppression in the putative RGC afferents compared with the simultaneously recorded dLGN relay cells (Figs. 3*E*,*F*, 4*F*,*G*). This is consistent with an enhanced inhibitory surround known to be present in the dLGN. Such a range of inputs to the dLGN is a parsimonious source of additional response features, such as an enhanced inhibitory field (Hubel and Wiesel, 1961; Singer, 1977; Sillito and Kemp, 1983; Webb et al., 2002; Bonin et al., 2005). Nevertheless, the broad pattern of asymmetries between ON and OFF cells was preserved for onset (Fig. 3), offset (Fig. 4), and latency measurements (Fig. 6), if not always significantly so. This reinforces the idea that the asymmetry between ON and OFF channels initiates in the retina (Zaidi et al., 2012; Li et al., 2017). However, the enhancement of the inhibitory suppression in the dLGN amplifies the magnitude of the differences.

In conclusion, we have shown that the asymmetries for bright versus dark afterimages and ON versus OFF cell post-stimulus rebound responses are weak or not apparent at smaller sizes that do not fully engage the RF surround. This is best explained by considering the RF/perceptive-field surround antagonism as the critical factor in driving both the post-stimulus response and resultant perceptual afterimage asymmetries. The data strengthen previous studies, including our own, demonstrating the close correlation between neural RF mechanisms in early visual areas and the resultant perception. Future studies should aim to causally manipulate the antagonistic balance between excitation and inhibition in behaving subjects, to robustly interrogate how visual information processing bridges from neuronal mechanisms to perceptual outcomes.

References

Acuna-Goycolea C, Brenowitz SD, Regehr WG (2008) Active dendritic conductances dynamically regulate GABA release from thalamic interneurons. Neuron 57:420–431.

Agrillo C, Gori S, Beran MJ (2015) Do rhesus monkeys (*Macaca mulatta*) perceive illusory motion. Anim Cogn 18:895–910.

Agrochao M, Tanaka R, Salazar-Gatzimas E, Clark DA (2020) Mechanism for analogous illusory motion perception in flies and humans. Proc Natl Acad Sci USA 117:23044–23053.

Allman J, Miezin F, Mcguinness E (1985) Stimulus specific responses from beyond the classical receptive field: neurophysiological mechanisms for local-global comparisons in visual neurons. Annu Rev Neurosci 8:407–430.

Angelucci A, Sainsbury K (2006) Contribution of feedforward thalamic afferents and corticogeniculate feedback to the spatial summation area of macaque V1 and LGN. J Comp Neurol 498:330–351.

Awatramani GB, Slaughter MM (2000) Origin of transient and sustained responses in ganglion cells of the retina. J Neurosci 20:7087–7095.

Bååth R, Seno T, Kitaoka A (2014) Cats and illusory motion. Psychology 5:1131–1134.

Bachy R, Zaidi Q (2014) Factors governing the speed of color adaptation in foveal versus peripheral vision. J Opt Soc Am A Opt Image Sci Vis 31: A220-5.

Barlow HB (1953) Summation and inhibition in the frog's retina. J Physiol 119:69–88.

Barlow HB (1956) Retinal noise and absolute threshold. J Opt Soc Am 46:634–639.

Barlow HB (1972) Single units and sensation: a neuron doctrine for perceptual psychology. Perception 1:371–394.

Barlow HB, Hill RM (1963) Evidence for a physiological explanation of the waterfall phenomenon and figural after-effects. Nature 200:1345–1347.

Barlow HB, Fitzhugh R, Kuffler WW (1957) Dark adaptation, absolute threshold and Purkinje shift in single units of cat's retina. J Physiol 137:327–337.

Barlow HB, Levick WR, Yoon M (1971) Responses to single quanta of light in retinal ganglion cells of the cat. Vision Res Suppl 3:87–101.

Bidwell S (1897) On the negative after-images following brief retinal excitation. Proc R Soc Lond B Biol Sci 61:268–271.

Bonin V, Mante V, Carandini M (2005) The suppressive field of neurons in lateral geniculate nucleus. J Neurosci 25:10844–10856.

Briggs F, Usrey WM (2009) Parallel processing in the corticogeniculate pathway of the macaque monkey. Neuron 62:135–146.

Buchner A, Baumgartner N (2007) Text: background polarity affects performance irrespective of ambient illumination and colour contrast. Ergonomics 50:1036–1063.

Budd JM (2004) How much feedback from visual cortex to lateral geniculate nucleus in cat: a perspective. Vis Neurosci 21:487–500.

Buldyrev I, Taylor WR (2013) Inhibitory mechanisms that generate centre and surround properties in ON and OFF brisk-sustained ganglion cells in the rabbit retina. J Physiol 591:303–325.

Chichilnisky EJ, Kalmar RS (2002) Functional asymmetries in ON and OFF ganglion cells of primate retina. J Neurosci 22:2737–2747.

Cleland BG, Lee BB (1985) A comparison of visual responses of cat lateral geniculate nucleus neurones with those of ganglion cells afferent to them. J Physiol 369:249–268.

Crandall SR, Cox CL (2012) Local dendrodendritic inhibition regulates fast synaptic transmission in visual thalamus. J Neurosci 32:2513–2522.

Dacey DM, Petersen MR (1992) Dendritic field size and morphology of midget and parasol ganglion cells of the human retina. Proc Natl Acad Sci USA 89:9666–9670.

Datskovskaia A, Carden WB, Bickford ME (2001) Y retinal terminals contact interneurons in the cat dorsal lateral geniculate nucleus. J Comp Neurol 430:85–100.

Derrington AM, Fuchs AF (1979) Spatial and temporal properties of X and Y cells in the cat lateral geniculate nucleus. J Physiol 293:347–364.

Einevoll GT, Heggelund P (2000) Mathematical models for the spatial receptive-field organization of nonlagged X cells in dorsal lateral geniculate nucleus of cat. Vis Neurosci 17:871–885.

Einevoll GT, Plesser HE (2002) Linear mechanistic models for the dorsal lateral geniculate nucleus of cat probed using drifting-grating stimuli. PLoS Comput Biol 13:503–530.

Einevoll GT, Plesser HE (2012) Extended difference-of-Gaussians model incorporating cortical feedback for relay cells in the lateral geniculate nucleus of cat. Cogn Neurodyn 6:307–324.

Enroth-Cugell C, Robson JG (1966) The contrast sensitivity of retinal ganglion cells of the cat. J Physiol 187:517–552.

Erişir A, Van Horn SC, Sherman SM (1997) Relative numbers of cortical and brainstem inputs to the lateral geniculate nucleus. Proc Natl Acad Sci USA 94:1517–1520.

Freed MA (2017) Asymmetry between ON and OFF α ganglion cells of mouse retina: integration of signal and noise from synaptic inputs. J Physiol 595:6979–6991.

Funke K, Eysel UT (1998) Inverse correlation of firing patterns of single topographically matched perigeniculate neurons and cat dorsal lateral geniculate relay cells. Vis Neurosci 15:711–729.

Gauthier JL, Field GD, Sher A, Shlens J, Greschner M, Litke AM, Chichilnisky EJ (2009) Uniform signal redundancy of parasol and midget ganglion cells in primate retina. J Neurosci 29:4675–4680.

Geisler WS (2008) Visual perception and the statistical properties of natural scenes. Annu Rev Psychol 59:167–192.

Gori S, Agrillo C, Dadda M, Bisazza A (2014) Do fish perceive illusory motion. Sci Rep 4:6443.

Hamos JE, Van Horn SC, Raczkowski D, Uhlrich DJ, Sherman SM (1985) Synaptic connectivity of a local circuit neurone in lateral geniculate nucleus of the cat. Nature 317:618–621.

Han C, Wang T, Wu Y, Li Y, Yang Y, Li L, Wang Y, Xing D (2021) The generation and modulation of distinct gamma oscillations with local, horizontal, and feedback connections in the primary visual cortex: a model study on large-scale networks. Neural Plast 2021:8874516.

Hartline HK (1940) The effects of spatial summation in the retina on the excitation of the fibers of the optic nerve. Am J Physiol 130:700–711.

Hochstein S, Shapley RM (1976) Linear and nonlinear spatial subunits in Y cat retinal ganglion cells. J Physiol 262:265–284.

Huang X, Levine S, Paradiso MA (2008) Rebounding V1 activity and a new visual aftereffect. J Vis 8:25–2510.

Hubel DH, Wiesel TN (1961) Integrative action in the cat's lateral geniculate body. J Physiol 155:385–398.

Hubel DH, Wiesel TN (1962) Receptive fields, binocular interaction and functional architecture in the cat's visual cortex. J Physiol 160:106–154.

Ikeda H, Wright MJ (1972) Receptive field organization of 'sustained' and 'transient' retinal ganglion cells which subserve different function roles. J Physiol 227:769–800.

Jansen M, Jin J, Li X, Lashgari R, Kremkow J, Bereshpolova Y, Swadlow HA, Zaidi Q, Alonso JM (2019) Cortical balance between ON and OFF visual responses is modulated by the spatial properties of the visual stimulus. Cereb Cortex 29:336–355.

Jin J, Weng C, Yeh CI, Gordon J, Ruthazer E, Stryker M, Swadlow H, Alonso JM (2008) ON and OFF domains of geniculate afferents in cat primary visual cortex. Nat Neurosci 11:88–94.

Jin J, Wang Y, Lashgari R, Swadlow HA, Alonso JM (2011) Faster thalamocortical processing for dark than light visual targets. J Neurosci 31:17471–17479.

Jones HE, Andolina IM, Oakely NM, Murphy PC, Sillito AM (2000) Spatial summation in lateral geniculate nucleus and visual cortex. Exp Brain Res 135:279–284.

Jung R (1973) Visual perception and neurophysiology. In: Handbook of sensory physiology: a central visual information, pp 1–152. Berlin: Springer.

Jung R, Spillmann L (1970) Receptive-field estimation and perceptual integration in human vision. In: Early experience and visual information processing in perceptual and reading disorders (Young FA, Lindsley DB, eds), pp 181–197. Washington, DC: National Academy of Sciences.

Khani A, Mustafar F, Rainer G (2018) Distinct frequency specialization for detecting dark transients in humans and tree shrews. Cell Rep 23:2405–2415.

Kleiner M, Brainard DH, Pelli D, Ingling A, Murray R, Broussard C (2007) What's new in Psychtoolbox-3. Perception 36.

Komban SJ, Alonso JM, Zaidi Q (2011) Darks are processed faster than lights. J Neurosci 31:8654–8658.

Komban SJ, Kremkow J, Jin J, Wang Y, Lashgari R, Li X, Zaidi Q, Alonso JM (2014) Neuronal and perceptual differences in the temporal processing of darks and lights. Neuron 82:224–234.

Kremkow J, Jin J, Komban SJ, Wang Y, Lashgari R, Li X, Jansen M, Zaidi Q, Alonso JM (2014) Neuronal nonlinearity explains greater visual spatial resolution for darks than lights. Proc Natl Acad Sci USA 111:3170–3175.

Kuffler SW (1953) Discharge patterns and functional organization of mammalian retina. J Neurophysiol 16:37–68.

Law CT, Gold JI (2010) Shared mechanisms of perceptual learning and decision making. Top Cogn Sci 2:226–238.

Li H, Liu X, Andolina IM, Li X, Lu Y, Spillmann L, Wang W (2017) Asymmetries of dark and bright negative afterimages are paralleled by subcortical ON and OFF poststimulus responses. J Neurosci 37:1984–1996.

Liang Z, Freed MA (2010) The ON pathway rectifies the OFF pathway of the mammalian retina. J Neurosci 30:5533–5543.

Liang Z, Freed MA (2012) Cross inhibition from ON to OFF pathway improves the efficiency of contrast encoding in the mammalian retina. J Neurophysiol 108:2679–2688.

Lindström S, Wróbel A (2011) Feedforward and recurrent inhibitory receptive fields of principal cells in the cat's dorsal lateral geniculate nucleus. Pflugers Arch 461:277–294.

Liu XB, Jones EG (1999) Predominance of corticothalamic synaptic inputs to thalamic reticular nucleus neurons in the rat. J Comp Neurol 414:67–79.

Luo J, He K, Andolina IM, Li X, Yin J, Chen Z, Gu Y, Wang W (2019) Going with the flow: the neural mechanisms underlying illusions of complex-flow motion. J Neurosci 39:2664–2685.

Macknik SL, Livingstone MS (1998) Neuronal correlates of visibility and invisibility in the primate visual system. Nat Neurosci 1:144–149.

Margolis DJ, Detwiler PB (2007) Different mechanisms generate maintained activity in ON and OFF retinal ganglion cells. J. Neurosci 27:5994–6005.

Mastronarde DN (1987a) Two classes of single-input X cells in cat lateral geniculate nucleus. I. Receptive-field properties and classification of cells. J Neurophysiol 57:357–380.

Mastronarde DN (1987b) Two classes of single-input X cells in cat lateral geniculate nucleus. II. Retinal inputs and the generation of receptive-field properties. J Neurophysiol 57:381–413.

Mazade R, Jin J, Pons C, Alonso JM (2019) Functional specialization of ON and OFF cortical pathways for global-slow and local-fast vision. Cell Rep 27:2881–2894.e5.

Mobarhan MH, Halnes G, Martínez-Cañada P, Hafting T, Fyhn M, Einevoll GT (2018) Firing-rate based network modeling of the dLGN circuit: effects of cortical feedback on spatiotemporal response properties of relay cells. PLoS Comput Biol 14:e1006156.

Montero VM (1986) Localization of gamma-aminobutyric acid (GABA) in type 3 cells and demonstration of their source to F2 terminals in the cat lateral geniculate nucleus: a Golgi-electron-microscopic GABA-immunocytochemical study. J Comp Neurol 254:228–245.

Montero VM (1987) Ultrastructural identification of synaptic terminals from the axon of type 3 interneurons in the cat lateral geniculate nucleus. J Comp Neurol 264:268–283.

Murphy PC, Duckett SG, Sillito AM (1999) Feedback connections to the lateral geniculate nucleus and cortical response properties. Science 286:1552–1554.

Murphy PC, Duckett SG, Sillito AM (2000) Comparison of the laminar distribution of input from areas 17 and 18 of the visual cortex to the lateral geniculate nucleus of the cat. J Neurosci 20:845–853.

Najafi F, Churchland AK (2018) Perceptual decision-making: a field in the midst of a transformation. Neuron 100:453–462.

Nolt MJ, Kumbhani RD, Palmer LA (2004) Contrast-dependent spatial summation in the lateral geniculate nucleus and retina of the cat. J Neurophysiol 92:1708–1717.

Norheim ES, Wyller J, Nordlie E, Einevoll GT (2012) A minimal mechanistic model for temporal signal processing in the lateral geniculate nucleus. Cogn Neurodyn 6:259–281.

Oehler R (1985) Spatial interactions in the rhesus monkey retina: a behavioural study using the Westheimer paradigm. Exp Brain Res 59:217–225.

Ono F, Kawahara JI (2007) The subjective size of visual stimuli affects the perceived duration of their presentation. Percept Psychophys 69:952–957.

Parker AJ, Newsome WT (1998) Sense and the single neuron: probing the physiology of perception. Annu Rev Neurosci 21:227–277.

Phillips I (2013) Afterimages and sensation. Philos Phenomenol Res 87:417–453.

Piscopo DM, El-Danaf RN, Huberman AD, Niell CM (2013) Diverse visual features encoded in mouse lateral geniculate nucleus. J Neurosci 33:4642–4656.

Prins N, Kingdom FA (2018) Applying the model-comparison approach to test specific research hypotheses in psychophysical research using the Palamedes Toolbox. Front Psychol 9:1250.

Rammsayer TH, Verner M (2014) The effect of nontemporal stimulus size on perceived duration as assessed by the method of reproduction. J Vis 14:17.

Ransom-Hogg A, Spillmann L (1980) Perceptive field size in fovea and periphery of the light- and dark-adapted retina. Vision Res 20:221–228.
Ratliff CP, Borghuis BG, Kao YH, Sterling P, Balasubramanian V (2010) Retina is structured to process an excess of darkness in natural scenes. Proc Natl Acad Sci USA 107:17368–17373.
Ravi S, Ahn D, Greschner M, Chichilnisky EJ, Field GD (2018) Pathway-specific asymmetries between ON and OFF visual signals. J Neurosci 38:9728–9740.
Rekauzke S, Nortmann N, Staadt R, Hock HS, Schöner G, Jancke D (2016) Temporal asymmetry in dark–bright processing initiates propagating activity across primary visual cortex. J Neurosci 36:1902–1913.
Rodieck RW (1965) Quantitative analysis of cat retinal ganglion cell response to visual stimuli. Vision Res 5:583–601.
Ruksenas O, Fjeld IT, Heggelund P (2000) Spatial summation and center-surround antagonism in the receptive field of single units in the dorsal lateral geniculate nucleus of cat: comparison with retinal input. Vis Neurosci 17:855–870.
Santacà M, Miletto Petrazzini ME, Agrillo C, Wilkinson A (2019) Can reptiles perceive visual illusions? Delboeuf illusion in red-footed tortoise (*Chelonoidis carbonaria*) and bearded dragon (*Pogona vitticeps*). J Comp Psychol 133:419–427.
Sceniak MP, Hawken MJ, Shapley R (2001) Visual spatial characterization of macaque V1 neurons. J Neurophysiol 85:1873–1887.
Schiller PH (1992) The ON and OFF channels of the visual system. Trends Neurosci 15:86–92.
Schiller PH (1995) The ON and OFF channels of the mammalian visual system. Prog Retin Eye Res 15:173–195.
Schiller PH, Dolan RP (1994) Visual aftereffects and the consequences of visual-system lesions on their perception in the rhesus-monkey. Vis Neurosci 11:643–665.
Schwabe L, Obermayer K, Angelucci A, Bressloff PC (2006) The role of feedback in shaping the extra-classical receptive field of cortical neurons: a recurrent network model. J Neurosci 26:9117–9129.
Sherman SM (2004) Interneurons and triadic circuitry of the thalamus. Trends Neurosci 27:670–675.
Sherman SM, Guillery RW (2002) The role of the thalamus in the flow of information to the cortex. Philos Trans R Soc Lond B Biol Sci 357:1695–1708.
Sillito AM, Jones HE (2008) The role of the thalamic reticular nucleus in visual processing. Thalamus & Related Systems 4:1–12.
Sillito AM, Kemp JA (1983) The influence of GABAergic inhibitory processes on the receptive field structure of X and Y cells in cat dorsal lateral geniculate nucleus (dLGN). Brain Res 277:63–77.
Singer W (1977) Control of thalamic transmission by corticofugal and ascending reticular pathways in the visual system. Physiol Rev 57:386–420.
Singer W, Creutzfeldt OD (1970) Reciprocal lateral inhibition of ON- and OFF-center neurones in the lateral geniculate body of the cat. Exp Brain Res 10:311–330.
Spillmann L (2009) Phenomenology and neurophysiological correlations: two approaches to perception research. Vision Res 49:1507–1521.
Spillmann L (2014) Receptive fields of visual neurons: the early years. Perception 43:1145–1176.
Spillmann L, Werner JS (1990) Visual perception: the neurophysiological foundations. San Diego: Academic.
Spillmann L, Ransom-Hogg A, Oehler R (1987) A comparison of perceptive and receptive fields in man and monkey. Hum Neurobiol 6:51–62.
Spillmann L, Dresp-Langley B, Tseng CH (2015) Beyond the classical receptive field: the effect of contextual stimuli. J Vis 15:7.
Subramaniyan M, Ecker AS, Berens P, Tolias AS (2013) Macaque monkeys perceive the flash lag illusion. PLoS One 8:e58788.
Szenczi P, Velázquez-López ZI, Urrutia A, Hudson R, Bánszegi O (2019) Perception of the Delboeuf illusion by the adult domestic cat (Felis silvestris catus) in comparison with other mammals. J Comp Psychol 133:223–232.
Tasaka GI, Guenthner CJ, Shalev A, Gilday O, Luo L, Mizrahi A (2018) Genetic tagging of active neurons in auditory cortex reveals maternal plasticity of coding ultrasonic vocalizations. Nat Commun 9:871.
Thoreson WB, Mangel SC (2012) Lateral interactions in the outer retina. Prog Retin Eye Res 31:407–441.
Uhlrich DJ, Cucchiaro JB, Humphrey AL, Sherman SM (1991) Morphology and axonal projection patterns of individual neurons in the cat perigeniculate nucleus. J Neurophysiol 65:1528–1541.
Uhlrich DJ, Cucchiaro JB (1992) GABAergic circuits in the lateral geniculate nucleus of the cat. In: Mechanisms of GABA action in the visual system: progress in brain research (Mize RR, Marc R, Sillito AM, eds), pp 171–192. Amsterdam: Elsevier.
Uhlrich DJ, Manning KA, Feig SL (2003) Laminar and cellular targets of individual thalamic reticular nucleus axons in the lateral geniculate nucleus in the prosimian primate Galago. J Comp Neurol 458:128–143.
Usrey WM, Reppas JB, Reid RC (1999) Specificity and strength of retinogeniculate connections. J Neurophysiol 82:3527–3540.
Van Horn SC, Eriş ir A, Sherman SM (2000) Relative distribution of synapses in the A-laminae of the lateral geniculate nucleus of the cat. J Comp Neurol 416:509–520.
Wang XX, Jin Y, Sun H, Ma C, Zhang J, Wang M, Chen L (2016) Characterization of rebound depolarization in neurons of the rat medial geniculate body in vitro. Neurosci Bull 32:16–26.
Webb BS, Tinsley CJ, Barraclough NE, Easton A, Parker A, Derrington AM (2002) Feedback from V1 and inhibition from beyond the classical receptive field modulates the responses of neurons in the primate lateral geniculate nucleus. Vis Neurosci 19:583–592.
Whittle P (1986) Increments and decrements: luminance discrimination. Vision Res 26:1677–1691.
Wu J, Liang Y, Chen S, Hsu CL, Chavarha M, Evans SW, Shi D, Lin MZ, Tsia KK, Ji N (2020) Kilohertz two-photon fluorescence microscopy imaging of neural activity in vivo. Nat Methods 17:287–290.
Wu Y, Dal Maschio M, Kubo F, Baier H (2020) An optical illusion pinpoints an essential circuit node for global motion processing. Neuron 108:722–734.e5.
Xing D, Yeh CI, Gordon J, Shapley RM (2014) Cortical brightness adaptation when darkness and brightness produce different dynamical states in the visual cortex. Proc Natl Acad Sci USA 111:1210–1215.
Xing D, Yeh CI, Shapley RM (2010) Generation of black-dominant responses in V1 cortex. J Neurosci 30:13504–13512.
Yeh CI, Xing D, Shapley RM (2009) Black responses dominate macaque primary visual cortex v1. J Neurosci 29:11753–11760.
Yousif N, Denham M (2007) The role of cortical feedback in the generation of the temporal receptive field responses of lateral geniculate nucleus neurons: a computational modelling study. Biol Cybern 97:269–277.
Zaghloul KA, Boahen K, Demb JB (2003) Different circuits for ON and OFF retinal ganglion cells cause different contrast sensitivities. J Neurosci 23:2645–2654.
Zaidi Q, Ennis R, Cao D, Lee B (2012) Neural locus of color afterimages. Curr Biol 22:220–224.
Zurawel G, Ayzenshtat I, Zweig S, Shapley RM, Slovin H (2014) A contrast and surface code explains complex responses to black and white stimuli in V1. J Neurosci 34:14388–14402.